American Society of Hematology
2021 L Street NW, Suite 900,
Washington, DC 20036
Phone: 202-776-0544 | Fax 202-776-0545
editorial@hematology.org

# Regulation of lymphoid-myeloid lineage bias through Regnase-1/3-mediated control of Nfkbiz

Tracking no: BLD-2023-020903R2

Takuya Uehata (Kyoto University, Japan) Shinnosuke Yamada (Kyoto University, Japan) Daisuke Ori (Kyoto University, Japan) Alexis Vandenbon (Kyoto University, Japan) amir giladi (Weizmann Institute of Science, Israel) Adam Jelinski (Weizmann Institute of Science, Israel) Yasuhiro Murakawa (Kyoto University, Japan) Hitomi Watanabe (Kyoto University, Japan) Kazuhiro Takeuchi (Kyoto University, Japan) Kazunori Toratani (Graduate School of Medicine, Kyoto University, Japan) Takashi Mino (Kyoto University, Japan) Hisanori Kiryu (The University of Tokyo, Japan) Daron Standley (Osaka university, Japan) Tohru Tsujimura (Hyogo Medical University, Japan) Tomokatsu Ikawa (Tokyo University of Science, Japan) Gen Kondoh (Kyoto University, Japan) Markus Landthaler (Max Delbrück Center for Molecular Medicine, Germany) Hiroshi Kawamoto (Institute for Life and Medical Sciences, Kyoto University, Japan) Hans-Reimer Rodewald (DKFZ, Germany) Ido Amit (Weizmann Institute of Science, Israel) Ryo Yamamoto (Kyoto University, Japan) Masaki Miyazaki (Institute for Life and Medical Sciences, Kyoto University, Japan) Osamu Takeuchi (Kyoto University, Japan)

**Abstract:**
**Regulation of lineage biases in hematopoietic stem and progenitor cells (HSPCs) is pivotal for balanced hematopoietic output. However, little is known about the mechanism behind lineage choice in HSPCs. Here, we show that mRNA decay factors Regnase-1 (Reg1; Zc3h12a) and Regnase-3 (Reg3; Zc3h12c) are essential for determining lymphoid fate and restricting myeloid differentiation in HSPCs. Loss of *Reg1* and *Reg3* resulted in severe impairment of lymphopoiesis and a mild increase in myelopoiesis in the BM. single cell RNA sequencing analysis (scRNA-seq) revealed that Reg1 and Reg3 regulate lineage directions in HSPCs via the control of a set of myeloid-related genes. Reg1- and Reg3-mediated control of mRNA encoding *Nfkbiz*, a transcriptional and epigenetic regulator, was essential for balancing lymphoid/myeloid lineage output in HSPCs *in vivo*. Furthermore, single cell-assay for transposase-accessible chromatin sequencing (scATAC-seq) analysis revealed that Reg1 and Reg3 control the epigenetic landscape on myeloid-related gene loci in early-stage HSPCs via *Nfkbiz*. Consistently, an antisense oligonucleotide designed to inhibit Reg1- and Reg3-mediated *Nfkbiz* mRNA degradation primed HSCs toward myeloid lineages by enhancing *Nfkbiz* expression. Collectively, the collaboration between post-transcriptional control and chromatin remodeling by the Reg1/Reg3-*Nfkbiz* axis governs HSPC lineage biases, ultimately dictating the fate of lymphoid versus myeloid differentiation.**

**Conflict of interest:** No COI declared

**COI notes:**

**Preprint server:** No;

**Author contributions and disclosures:** T.U. and O.T. were in charge of experimental designs, analyses, interpretation of data and drafting of the manuscript; S.Y., D.O., K.T., and M.M. participated in the acquisition, analysis and interpretation of data; A.J., A.G., and I.A. handled scRNA-seq samples and performed analyses on scRNA-seq data. A.V. and K.T. performed analysis of scRNA-seq and scATAC-seq data; Y.M. and M.L. performed HITS-CLIP of Regnase-3; H.K. analyzed HITS-CLIP of Regnase-1 and Regnase-3; H.W. and G.K. contributed to genetic engineering to generate multiple mouse lines; T.T. performed histological examination; T.I. and R.Y. contributed to in vitro culture of multipotent progenitors and HSCs, respectively; D.M.S. carried out structural modeling; T.M., M.M., R.Y., H.R.R., and H.K. provided critical discussions and suggestions; O.T. supervised the overall study.

**Non-author contributions and disclosures:** No;

**Agreement to Share Publication-Related Data and Data Sharing Statement:** scRNA-seq data and scATAC-seq data have been deposited in the NCBI's GEO under accession code GSE228923 and GSE229065, respectively.

**Clinical trial registration information (if any):**

# Regulation of lymphoid-myeloid lineage bias through Regnase-1/3-mediated control of Nfkbiz

**Running title:** The Regnase-1/3-Nfkbiz axis shapes HSPC lineages

Takuya Uehata[1,11], Shinnosuke Yamada[1,11], Daisuke Ori[1,12], Alexis Vandenbon[3], Amir Giladi[2], Adam Jelinski[2], Yasuhiro Murakawa[4], Hitomi Watanabe[3], Kazuhiro Takeuchi[4], Kazunori Toratani[1], Takashi Mino[1], Hisanori Kiryu[5], Daron M. Standley[6], Tohru Tsujimura[7], Tomokatsu Ikawa[8], Gen Kondoh[3], Markus Landthaler[9], Hiroshi Kawamoto[3], Hans-Reimer Rodewald[10], Ido Amit[2], Ryo Yamamoto[4], Masaki Miyazaki[3], Osamu Takeuchi[1,*]

[1]Laboratory of Medical Chemistry, Graduate School of Medicine, Kyoto University; Kyoto, Japan

[2]Department of Immunology, Weizmann Institute of Science; Rehovot, Israel

[3]Institute for Life and Medical Sciences, Kyoto University; Kyoto, Japan

[4]Institute for the advanced study of human biology, Kyoto University; Kyoto, Japan.

[5]Department of Computational Biology and Medical Sciences, Graduate School of Frontier Sciences, The University of Tokyo; Chiba, Japan

[6]Department of Genome Informatics, Genome Information Research Center, Research Institute for Microbial Diseases (RIMD), Osaka University; Osaka, Japan

[7]Department of Pathology, Hyogo College of Medicine; Hyogo, Japan

[8]Division of Immunology and Allergy, Research Institute for Biomedical Sciences, Tokyo University of Science; Chiba, Japan

[9]RNA Biology and Posttranscriptional Regulation, Max Delbrück Center for Molecular Medicine Berlin, Berlin Institute for Molecular Systems Biology; Berlin, Germany

[10]German Cancer Research Center (DKFZ); Heidelberg, Germany

[11]These authors contributed equally

[12]Present address: Laboratory of Molecular Immunobiology, Division of Biological Science, Graduate School of Science and Technology, Nara Institute of Science and Technology (NAIST), 8916-5 Takayama-cho, Ikoma, Nara, 630-0192, Japan

Correspondence: Osamu Takeuchi, Laboratory of Medical Chemistry, Graduate School of Medicine, Kyoto University, Yoshida-Konoe-cho, Sakyo-ku, Kyoto 606-8501, Japan; e-mail: otake@mfour.med.kyoto-u.ac.jp.

Data are available on request from the corresponding author, Osamu Takeuchi (otake@mfour.med.kyoto-u.ac.jp). scRNA-seq data and scATAC-seq data have been deposited in the NCBI's GEO under accession code GSE228923 and GSE229065, respectively. Mouse strains generated in this work are available for non-commercial research purposes following a reasonable request. Source data are provided with this paper.

Text, 3999 words

Abstract, 199 words

Figure 1-7

Supplemental Figures 1-10

Supplemental Table 1-6

reference 1-47

**Key Points**

- Regnase-1 and Regnase-3 are RNases critical for determining lymphoid fate and restricting myeloid differentiation in HSPCs.
- Regnase-1/3-mediated decay of *Nfkbiz*, an epigenetic regulator crucial for HSPC lineage choice, is potently manipulated by an ASO.

**Abstract**

**Regulation of lineage biases in hematopoietic stem and progenitor cells (HSPCs) is pivotal for balanced hematopoietic output. However, little is known about the mechanism behind lineage choice in HSPCs. Here, we show that mRNA decay factors Regnase-1 (Reg1; Zc3h12a) and Regnase-3 (Reg3; Zc3h12c) are essential for determining lymphoid fate and restricting myeloid differentiation in HSPCs. Loss of *Reg1* and *Reg3* resulted in severe impairment of lymphopoiesis and a mild increase in myelopoiesis in the BM. single cell RNA sequencing analysis (scRNA-seq) revealed that Reg1 and Reg3 regulate lineage directions in HSPCs via the control of a set of myeloid-related genes. Reg1- and Reg3-mediated control of mRNA encoding *Nfkbiz*, a transcriptional and epigenetic regulator, was essential for balancing lymphoid/myeloid lineage output in HSPCs *in vivo*. Furthermore, single cell-assay for transposase-accessible chromatin sequencing (scATAC-seq) analysis revealed that Reg1 and Reg3 control the epigenetic landscape on myeloid-related gene loci in early-stage HSPCs via *Nfkbiz*. Consistently, an antisense oligonucleotide designed to inhibit Reg1- and Reg3-mediated *Nfkbiz* mRNA degradation primed HSCs toward myeloid lineages by enhancing *Nfkbiz* expression. Collectively, the collaboration between post-transcriptional control and chromatin remodeling by the Reg1/Reg3-*Nfkbiz* axis governs HSPC lineage biases, ultimately dictating the fate of lymphoid versus myeloid differentiation.**

## Introduction

Hematopoietic stem and progenitor cells (HSPCs) in the bone marrow (BM) generate multi-lineages that contribute to the production of all mature blood and immune cells. This process is tightly controlled to maintain the balance between lymphoid, myeloid, erythroid and megakaryocytic cell populations under steady state conditions.[1-3] Consistent with the recent lineage-biased output model of HSPCs,[4-7] the pattern of gene expression in the progenitor reflects that of the mature cell type toward which it is biased, a phenomenon known as transcriptional lineage priming.[1,8,9] This is initiated by cell-intrinsic and -extrinsic factors, controlling lineage-determining transcription programs. Under microbial infection, inflammatory cytokines such as interleukin (IL)-1β and tumor necrosis factor (TNF) trigger reprograming of transcriptional networks in HSPCs to prime myelopoiesis by inducing the lineage-determining transcription factors (TFs) PU.1 and C/EBPβ.[10-17] In addition, alterations in epigenetic landscape can contribute to transcriptional lineage priming in a cell-intrinsic manner.[18-20] However, molecular mechanisms that explain the link between lineage output and transcriptional status need to be clarified.

Regnase-1 (Reg1) is an endoribonuclease that degrades mRNAs harboring stem-loop (SL) structures with a pyrimidine-purine-pyrimidine loop in the 3' untranslated regions (UTRs).[21-23] Regnase-1 is critical for the suppression of inflammatory responses in mature immune cells, and for the maintenance of immune homeostasis.[24,25] There are four Regnase family members (Reg1 to 4) in mammals characterized by the presence of an RNase domain and a CCCH-type zinc finger (Zf) domain. However, it remains unclear to what extent Regnase family members play redundant roles in the immune system.

In this study, we clarified the roles of Reg1 and Reg3 in HSPC lineage choice through the control of *Nfkbiz* mRNA stability. Further, we developed a method that induces HSC myeloid priming by using an antisense oligonucleotide (ASO) which

inhibits Reg1/Reg3-mediated *Nfkbiz* degradation.

## Methods

### Single cell RNA-seq

Sc sorting for scRNA-seq was performed as previously described.[26,27] Briefly, $Lin^-$ cells were purified from mice competitively reconstituted with WT (CD45.1) and *DKO* (CD45.2) FL cells. WT and *DKO* LSK cells were sc-sorted into 384-well cell capture plates containing lysis solution and barcoded poly(T) reverse-transcription (RT) primers. Immediately after sorting, each plate was spun down to ensure cell immersion into the lysis solution, snap frozen on dry ice and stored at −80 °C until processed.

Full details are provided in the supplemental Methods.

## Results

### Reg1 and Reg3 are essential for balanced lineage output in BM

Among Regnase family members, lineage-negative ($Lin^-$) hematopoietic progenitor highly express Reg1 and Reg3 (supplemental Figure 1A-C). Therefore, we investigated whether Reg1 and Reg3 regulate hematopoietic differentiation in the BM. Since mice lacking both *Reg1* and *Reg3* (DKO), but not *Reg1* or *Reg3* alone (supplemental Figure 1C-E), exhibited perinatal lethality, accompanied by marked infiltration of neutrophils in the periportal region of the liver and the parenchyma of the pancreas (supplemental Figure 1F). To investigate hematopoiesis, we performed fetal liver (FL) transplantation using E15.5 fetuses of *Reg1*$^{-/-}$, *Reg3*$^{-/-}$, or *DKO* donors, and sacrificed them 4-6 weeks after transplantation. Interestingly, *DKO* FL-transplanted mice displayed a profound loss of $B220^+CD19^+$ B cells and a reciprocal increase in $CD11b^+$ myeloid cells in the peripheral blood compared to control (supplemental Figure 1G-H). In contrast, deficiency of *Reg1* or *Reg3* alone did not lead to profound changes in immune cells. Consistently, E15.5 *DKO* FL cells exhibited decreased B cells and increased myeloid cells (supplemental Figure 1I). These results suggest the redundant roles of Reg1 and Reg3 in hematopoiesis.

To investigate whether the influence of *Reg1/Reg3* deficiency on BM hematopoiesis is cell-intrinsic, we performed competitive FL transplants. We engrafted equal numbers of control or DKO FL cells (CD45.2) alongside competitor cells (CD45.1) into lethally irradiated recipient mice (CD45.1/45.2) (Figure 1A). We observed comparable engraftment levels in mice receiving control and DKO FL cells (supplemental Figure 2A). *DKO* FL-transplanted mice showed a significant reduction of B/T-lymphocytes and a concomitant increase in myeloid cells in the peripheral blood in the frequencies and numbers (Figure 1B-C). A similar trend was observed in the BM, marked by reduced B cell numbers and an increase in $Gr\text{-}1^+CD11b^+$ myeloid cells (supplemental Figure 2B-C). Consistently, Thymic T cell populations were reduced in

*DKO* mice compared to controls (supplemental Figure 2D). The analysis of BM hematopoietic progenitors in mixed chimera revealed that *DKO* cells failed to give rise to all B cell-lineage cells, and showed unimpaired or mildly increased proportion of megakaryocytic-erythroid and myeloid lineages (Figure 1D-F).

We then asked whether Reg1 and Reg3 were required for B-lymphopoiesis in uncommitted or lymphoid lineage-committed progenitor stages. To address this, we utilized *Il7r*-cre$^{+}$ROSA-YFP$^{+}$*Reg1*$^{fl/fl}$*Reg3*$^{-/-}$ mice (*DKO*$^{Il7r\text{-cre}}$), in which *Reg1* gene was deleted via *Il7r*-driven cre recombination. We confirmed *Il7r*-cre-mediated recombination at the pro-B stage and, to a lesser extent, the CLP based on RT-PCR for *Reg1* and YFP expression (supplemental Figure 2E-F). Through competitive FL transplantation experiments, we observed that B cell differentiation remained unchanged in YFP-expressing *DKO*$^{Il7r\text{-cre}}$ cells compared to their control counterparts (supplemental Figure 2G). These results indicate that Reg1 and Reg3 function at uncommitted stages of B-lymphopoiesis and become dispensable once the cells undergo lineage commitment.

To understand how Reg1 and Reg3 regulate BM hematopoiesis, we examined the proliferative activity and cell viability of uncommitted progenitors. *In vivo* BrdU incorporation experiments using mixed chimera receiving control and *DKO* FL cells showed no difference in proliferative activity of CD150$^{+}$ or $^{-}$ LSK, Flt3$^{+}$ MPP, CLP, or myeloid progenitors such as CMP, GMP, and MEP between these genotypes (Figure 1G). In addition, Annexin V$^{+}$ apoptotic cell frequencies were comparable between control and *DKO* (Figure 1H). These results suggest that Reg1 and Reg3 regulate lymphoid lineage differentiation, rather than affecting cell proliferation or viability.

To evaluate the roles of Reg1 and Reg3 in steady-state hematopoiesis, we generated *Reg1* conditional knockout mice crossed with *Reg3*$^{-/-}$ animals, utilizing tamoxifen-inducible cre recombinase system (supplemental Figure 3A-B). CreERT2$^{+}$*Reg1*$^{fl/fl}$*Reg3*$^{-/-}$ (*DKO*$^{CreERT2}$) mice also exhibited a reduction in B220$^{+}$CD19$^{+}$

B cells and an increase in $CD11b^+$ myeloid cells both in frequencies and numbers, at day 14 post-tamoxifen injection (supplemental Figure 3C-D). We next examined HSPC subpopulations defined as LT-HSC ($Flt3^-CD150^+CD48^-LSK$), ST-HSC ($Flt3^-CD150^-CD48^-LSK$), MPP2 ($Flt3^-CD150^+CD48^+LSK$), MPP3 ($Flt3^-CD150^-CD48^+LSK$), MPP4($Flt3^+CD150^-CD48^+LSK$), CLPs ($Flt3^+IL\text{-}7R\alpha^+Lin^-Sca1^{dull}Kit^{dull}$) (supplemental Figure 3E). *DKO*$^{CreERT2}$ mice displayed a significant reduction in CLPs, while ST-HSC, MPP2, and MPP3 showed increased numbers compared to control mice (supplemental Figure 3F-G).

Taken together, our findings suggest that Reg1 and Reg3 are important for balancing lymphoid-myeloid differentiation in HSPCs.

**Reg1 and Reg3 are required for the priming of lymphoid-biased HSPCs**

Recent scRNA-seq approaches suggest that transcriptional lineage priming is initiated in HSPCs and is correlated with their functional lineage biases.[1,15,26,28] To investigate if Reg1 and Reg3 contribute to shaping lineage biases in HSPCs, we performed scRNA-seq analysis of WT and *DKO* LSK cells containing HSCs and MPPs from competitively FL-transferred mice (Figure 2A). WT and *DKO* LSK populations were single cell-sorted into 384 well plates, and 2241 and 2242 cells were analyzed from each background, respectively (Figure 2B; supplemental Figure 4A). We utilized the MetaCell approach by which homologous populations were grouped based on similar transcriptional profiles to distinguish between closely related cell types (supplemental Figure 4B).[26] When WT and *DKO* cells were projected onto the hematopoietic core map,[26] *DKO* cells were enriched in the direction of myeloid and megakaryocytic-erythroid progenitors compared with control, whereas lymphoid lineages were underrepresented in *DKO* cells (Figure 2C). Consistently, meta-cells representing myeloid- and megakaryocitic/erythroid-biased populations increased in *DKO* samples compared to WT, while those representing lymphoid populations

decreased in *DKO* samples (Figure 2C-D; supplemental Figure 4C; supplementary Table 1). The expression levels of phenotypic markers for myeloid-biased HSCs, such as CD41, did not significantly increase in *DKO* cells (supplemental Figure 4D-F). Thus, our results support the notion that Reg1 and Reg3 are critical for the generation of B lymphoid lineages from HSCs to maintain balanced hematopoiesis.

### *DKO* HSCs shift toward myeloid-biased hematopoiesis upon serial transplantation

We further assessed the long-term maintenance of lineage-biased hematopoiesis in *DKO* HSCs by transplanting LT-HSCs isolated from CreERT2$^{+}$ control or CreERT2$^{+}$*Reg1*$^{fl/fl}$*Reg3*$^{-/-}$ mice (*DKO*$^{CreERT2}$) along with supportive BM cells into lethally irradiated recipients (supplemental Figure 5A). *DKO*$^{CreERT2}$ LT-HSCs gave rise to a higher percentage of granulocytes and monocytes and a lower percentage of B/T-lymphocytes compared to control after primary transplantation (supplemental Figure 5B). In secondary recipients, *DKO*$^{CreERT2}$ LT-HSC-derived cells maintained skewed lineage outputs toward granulocytes and monocytes, and away from B/T-lymphocytes, compared to control LT-HSC-derived cells (supplemental Figure 5C). Notably, the number of LT-HSCs was not altered 3 months after primary and secondary transplantation (supplemental Figure 5D-E). These finding indicate that myeloid-biased hematopoiesis persisted in the absence of *Reg1* and *Reg3* even after secondary transplantation.

### Reg1 and Reg3 cooperatively regulate a set of mRNAs including *Nfkbiz* and *Ehd3*

We next explored how degradation of a common set of mRNAs in HSCs allows Reg1 and Reg3 to prime and maintain B-lymphoid lineage-biased MPPs. We compared differentially expressed genes between WT and *DKO* HPSCs by reanalyzing the scRNA-seq data (supplementary Table 2). Remarkably, most of the upregulated genes in *DKO* cells were myeloid lineage-associated genes, such as *Mpo*, *Ccl9*, *Ctsg*, *Ebi3*, and

*Elane* (Figure 2F). In contrast, downregulated genes included *Dntt* and *Stmn1*, which are required for lymphoid development and suppression of megakaryocytic differentiation, respectively.[29,30] Consistently, *Mpo*, *Elane*, and *Ebi3* were highly expressed in myeloid and monocyte progenitors of *DKO* cells compared to WT counterparts (Figure 2G; supplemental Figure 6A). In addition to myeloid-associated genes, *Nfkbiz* and *Ehd3* were found to be upregulated in *DKO* cells (Figure 2F-G; supplemental Figure 6A). Interestingly, these genes were increased in *DKO* cells even in undetermined progenitors, which potentially contain HSCs, as well as lymphoid- and myeloid-biased progenitors (Figure 2G; supplemental Figure 6A). qPCR analysis using mixed chimera mice receiving WT and *DKO* FL cells confirmed a significant elevation of *Nfkbiz* and *Ehd3* in *DKO* $CD150^{+}$LSK and LMPP, compared with WT cells (supplemental Figure 6B). On the other hand, lineage-related TFs that can skew HSPC differentiation toward myeloid or megakaryocytic-erythroid lineages, including *Cebpa*, *Cebpb*, *Spi1*, and *Gata1*, were not altered between WT and *DKO* cells (supplemental Figure 6B).

Then, we examined if the genes increased in *DKO* HSPCs were directly controlled by these RNases. Luciferase reporter experiments showed that both Reg1 and Reg3 inhibited the luciferase activity in cells expressing luciferase constructs harboring 3'UTRs of *Nfkbiz* and *Ehd3* (Figure 2H). In contrast, nuclease-dead (ND) mutants of Reg1 (D141N) and Reg3 (D271N) failed to suppress the reporter activity, suggesting that Reg1 and Reg3 inhibited *Nfkbiz* and *Ehd3* in a manner dependent on their RNase enzymatic activities. 3'UTR of *Irf8* and *Cebpd* were also responsive to overexpression of Reg1 or Reg3, but no significant change in their gene expressions was observed in *DKO* progenitors (supplemental Figure 6B-C). However, *Reg1*/*Reg3*-doubly-deficient $Lin^{-}$ cells showed enhanced stability of *Nfkbiz* transcript and had only a partial effect on *Ehd3*, whereas the stability of *Irf8* or *Cebpd* mRNAs were not influenced by double-deficiency of *Reg1* and *Reg3* (Figure 2I; supplemental Figure 6D), confirming

that both Reg1 and Reg3 are required to downregulate or suppress *Nfkbiz* and *Ehd3* mRNA levels.

**Reg1 and Reg3 control lymphoid-myeloid lineage balance via *Nfkbiz* in HSPCs**

To investigate whether *Nfkbiz* or *Ehd3* influences lymphoid and/or myeloid differentiation in HSPCs, we employed a culture system of mouse primary MPPs maintained by overexpressing human Id3-ERT2 fusion protein (MPP$^{hId3\text{-}ERT2}$) in the presence of 4-hydroxytamoxifen (4-OHT) (Figure 3A).[31] We retrovirally expressed *Nfkbiz*, *Ehd3*, and TFs implicated in myeloid differentiation as controls in MPP$^{hId3\text{-}ERT2}$ cells. As expected, expression of myeloid master regulators, C/EBPα and C/EBPβ, strongly blocked B cell differentiation and induced myeloid differentiation (Figure 3B-C). Interestingly, Nfkbiz expression in MPP$^{hId3\text{-}ERT2}$ cells resulted in a profound defect in lymphoid differentiation and promoted myeloid lineage differentiation to a degree similar to the effects of C/EBPα and C/EBPβ, whereas Ehd3 showed only a modest effect on myeloid-lymphoid differentiation in MPP$^{hId3\text{-}ERT2}$ cells (Figure 3B-C). We then established MPP $^{hId3\text{-}ERT2}$ cells from *Reg1*$^{fl/fl}$*Reg3*$^{-/-}$ BM cells where cre recombinase could be expressed by doxycycline (DOX) treatment *in vitro* (tetO-*cre-Reg1*$^{fl/fl}$*Reg3*$^{-/-}$ MPP$^{hId3\text{-}ERT2}$) (supplemental Figure 7A-C). Consistent with the hematopoietic changes in the BM caused by double-deficiency of *Reg1* and *Reg3*, tetO-*cre-Reg1*$^{fl/fl}$*Reg3*$^{-/-}$ MPP$^{hId3\text{-}ERT2}$ cells failed to induce CD19$^{+}$ cells, but reciprocally increased CD11b$^{+}$ myeloid cells under B cell differentiating condition in the presence of DOX (Figure 3D). The Nfkbiz expression was strikingly elevated following *Reg1* depletion both at mRNA and protein levels (Figure 3E-F). RNA-immunoprecipitation (IP) experiments showed that ND mutants of Reg1 or Reg3 co-precipitated mRNA for *Nfkbiz*, but not a Reg1 non-target gene *Nfkbia* (Figure 3G-H), indicating that both Reg1 and Reg3 directly interact with *Nfkbiz* mRNA.

We then asked whether the lineage bias in hematopoiesis in the absence of *Reg1* and *Reg3* depends on *in vivo Nfkbiz* expression. For this purpose, we crossed *DKO*$^{CreERT2}$ mice, which showed elevated Nfkbiz expression in Lin$^-$ BM cells (supplemental Figure 7D), with *Nfkbiz*$^{fl/fl}$ (*TKO*$^{CreERT2}$) mice, and analyzed them at day14 post-tamoxifen injection. Intriguingly, *TKO*$^{CreERT2}$ mice showed a dramatic improvement in the frequencies and numbers of HSPC subpopulations compared to *DKO*$^{CreERT2}$ mice (Figure 4A-C). In parallel, the frequency and number of CD19$^+$B220$^+$ B cells, as well as CD11b$^+$ myeloid cells, were fully restored in *TKO*$^{CreERT2}$ mice (Figure 4D-I). Moreover, B cell differentiation potential was also restored in *TKO*$^{CreERT2}$ cells in an *in vitro* B cell differentiation assay (Figure 4J-L), indicating that the upregulation of Nfkbiz accounts for the alteration in HSC lineage determination under the *Reg1*/*Reg3* double-deficiency. Taken together, these findings demonstrate that the posttranscriptional control of *Nfkbiz* expression by Reg1 and Reg3 licenses lymphopoiesis by suppressing myeloid differentiation in HSPCs.

**The Reg1/Reg3-*Nfkbiz* axis shapes epigenetic lineage priming in HSC**

Since Nfkbiz acts as a transcriptional modulator inducing chromatin remodeling,[32,33] we hypothesized that the increased *Nfkbiz* expression modified epigenetic landscape in HSCs. To address this possibility, we examined the single-cell chromatin accessibility landscape using scATAC-seq of Flt3$^-$CD48$^-$ LSK population, which contains HSCs and the intermediate cells between HSCs and CD48-positive lineage-biased MPPs (Figure 5A).[34,35] We sequenced 13859, 9936, 10991, and 6902 cells for control, *Nfkbiz*$^{CreERT2}$, *DKO*$^{CreERT2}$, and *TKO*$^{CreERT2}$, respectively. UMAP plot for total cells showed that clustering based on the differential chromatin accessibilities generated 18 clusters (C1-C18) (Figure 5B). To dissect the chromatin accessibility profiles across the clusters, we examined the selected markers for HSCs and mature cell lineages.[26,36] The chromatin of stemness-related genes (*Hoxa9, Hoxa10, Gata2, Mllt3, Hlf, Meis1*, and

*Msi2*) was more accessible in clusters C1-C8 compared with the rest of the clusters (Figure 5C; supplemental Figure 8A-C). In contrast, C10-C14 clusters displayed distinct patterns of accessibilities in a set of myeloid-related genes (*Spi1*, *Csf1r*, *Csf2rb*, *Csf3r*, *F13a1*, and *Fcer1g*) and lymphoid-related genes (*Flt3* and *Satb1*) (Figure 5C; supplemental Figure 8A-C), suggesting that cells in these clusters harbor myeloid/lymphoid epigenetic features reminiscent of MPP5 and MPP6 that are phenotypically defined as $CD34^{-}$ and $CD34^{+}$ $Flt3^{-}CD150^{-}CD48^{-}$ LSK, respectively.[35] Among C1-C8, C1-C5 were consolidated in the UMAP plot and showed common features in the increased accessibility of lymphoid- and myeloid-related genes compared to C6-C8 (Figure 5B-C). In contrast, erythroid-related genes (*Gata1*, *Epor*, and *Car1*) were accessible in C6-C8 (Figure 5C).

The chromatin accessibility landscape was dramatically altered in $DKO^{CreERT2}$ cells characterized by their dominance in C3 and C8 together with the underrepresentation of C1, C2, C4, C5 and C7 (Figure 5D-E). In contrast, $DKO^{CreERT2}$ cells were evenly observed in C10-C14. Interestingly, $DKO^{CreERT2}$ cells showed more accessibility for myeloid-related genes such as *Cd74* and *Csf2rb* than control in C1-C8 (Figure 5C,F). Notably, the changes in chromatin accessibility in *DKO* cells were drastically restored by further deletion of *Nfkbiz*, implying that Reg1 and Reg3 regulate epigenetic homeostasis in HSCs by suppressing the expression of *Nfkbiz* (Figure 5D-F).

Consistent with the role of Nfkbiz in controlling gene expression via interaction with TFs like NF-κB, NFKB-binding motifs were enriched in regions more accessible in $DKO^{CreERT2}$ cells compared to control cells in C1-C5 clusters (Figure 5G). Further, GATA and IRF family-binding motifs were also more frequently observed in regions highly accessible in $DKO^{CreERT2}$ cells in C1-C5 and C6-C8 clusters, respectively (Figure 5G-H). These findings suggest that the activation of Nfkbiz in $DKO^{CreERT2}$ cells can facilitate the recruitment of TFs involved in lineage priming via chromatin remodeling.

**Reg3 and Reg1 recognize and destabilize mRNAs with common signatures**

Next, we analyzed the mechanisms how Reg1 and Reg3 recognize target mRNAs. Since Reg1-interacting stem-loop motifs were identified by high-throughput sequencing of crosslinking and IP (HITS-CLIP) analyses,[23] we analyzed the transcriptome-wide binding mode of Reg3 with the same technique. To this end, HEK293T cells stably expressing DOX-inducible FLAG-tagged Reg3 were generated and UV crosslinked. IP of FLAG-Reg3 yielded Reg3-RNA complexes following induction of Reg3 by DOX treatment (Figure 6A). Recovered RNA fragments from two independent HITS-CLIP experiments were deep-sequenced, and genome-aligned reads were clustered, allowing identification of 6639 and 7678 putative Reg3-binding sites in two biological duplicate libraries, respectively (Supplementary Table 3). We found that the uniquely-mapped reads of Reg3-binding sites were enriched in 3' UTRs (Figure 6B). When the secondary structures of these sequences were analyzed by RNAfold,[37] SL structures with 3-7 nucleotide stems and tri-nucleotide loops were significantly enriched (Figure 6C). In addition, motif analyses of the SL sequences revealed that the UAU triplet was overrepresented in the hairpin sequences of Reg3-binding motifs (Figure 6D). This is reminiscent of Reg1-binding motifs revealed by HITS-CLIP analysis (Figure 6E-F).[23] Interestingly, Reg3- and Reg1-binding sequences overlapped significantly (Supplementary Table 4), indicating that Reg3 and Reg1 target an overlapping set of mRNAs by recognizing a common binding motif.

Consistently, a luciferase reporter RNA harboring the SL-containing sequence with an UAU-loop sequence in the 3' UTR was suppressed by the overexpression of either RNase-competent Reg3 or Reg1 (Figure 6G-H). Disruption of the SL structure by mutating either side of the stem sequence abrogated the Reg3-mediated suppression of the luciferase activity (Figure 6G-H). Restoration of the SL structure by mutating both sides of the stem sequences restored Reg3 responsiveness (Figure 6H). SLs harboring

UAU and, to a lesser extent, UGU, but not ACA, AAA or UCU, were suppressed by Reg3, suggesting that the pyrimidine-purine-pyrimidine loop sequences are required for Reg3 suppression, similar to Reg1 (Figure 6I). These results demonstrate that Reg3 and Reg1 recognize overlapping sets of mRNAs by recognizing common SL sequences present in the mRNA 3' UTR.

Next, we investigated SL structure(s) in *Nfkbiz* 3'UTR responsible for the Reg1/Reg3-mediated decay. Luciferase reporter assays revealed that the *Nfkbiz* instability element was located within the 1-200 region of its 3'UTR and contains 4 SL structures (SL1-4) (supplemental Figure 9A-B). Among these, SL3 and SL4, but not SL1 and SL2, were responsible for the suppression by both Reg1 and Reg3 (supplemental Figure 9C). These SLs harbor UAU-loop sequences (supplemental Figure 9B), a consensus motif for Reg1 and Reg3 recognition (Figure 6D,F). Consistently, a reporter containing either SL3 or SL4 was suppressed by the overexpression of Reg1 or Reg3 (supplemental Figure 9D). The Reg1/Reg3 responsiveness of SL3 and SL4 was abrogated by mutation of SL structures and was rescued by restoration of SL structures by introducing mutations in both sides of the stem sequences (Figure 6J-K), indicating that Reg1 and Reg3 commonly recognize SL structures in SL3 and SL4 for degrading *Nfkbiz*.

**Enhancement of *Nfkbiz* expression via its 3'UTR leads to myeloid priming in HSCs**

The aforementioned results prompted us to hypothesize that enhancement of *Nfkbiz* expression by inhibiting Reg1/Reg3-mediated decay could control HSC lineage bias. We achieved an increase in Reg1 expression by targeting its self-regulation through the use of ASOs against SL structures located in the *Reg1* 3' UTR.[38] To inhibit Reg1/Reg3-mediated *Nfkbiz* mRNA decay, we designed morpholino ASOs to target and disrupt the SL structures of SL1, SL2, and SL3-4 (supplemental Figure 9B). Since SL3 and SL4 aligned tandemly with a short interval, we designed an ASO targeting both SL3

and SL4 (Figure 7A). When we introduced ASOs together with the reporter harboring the full-length *Nfkbiz* 3'UTR, the SL3-4-targeting ASO highly increased luciferase activity compared to control-oligo or ASOs against SL1 or SL2 (Supplemental Figure 10A). The results suggest that the SL3-4-targeting ASO (hereafter *Nfkbiz*-ASO) is potent to stabilize *Nfkbiz* mRNA by altering the SL structure. Likewise, in BM-derived macrophages, the *Nfkbiz*-ASO stabilized *Nfkbiz* mRNA and enhanced *Nfkbiz* expression both at the mRNA and protein levels (supplemental Figure 10B-D). Consistent with the pro-inflammatory function of Nfkbiz in macrophages, the *Nfkbiz*-ASO augmented IL-6 production following LPS treatment (supplemental Figure 10E). In contrast, *Nfkbiz*-ASO failed to increase *Nfkbiz* expression in *Reg1/Reg3 DKO* macrophages (supplemental Figure 10F), suggesting that the ASO enhanced *Nfkbiz* expression by inhibiting Reg1/Reg3-mediated mRNA decay.

Next we investigated if the *Nfkbiz*-ASO is also potent to increase the *Nfkbiz* expression in HSC by using a serum-free HSC culture system that enables efficient enrichment of $CD150^{+}CD48^{-}CD201^{+}$LSK population (Figure 7B; supplemental Figure 10G-H).[39] We found that a FITC-conjugated ASO was efficiently introduced into cultured HSCs (cHSCs) by electroporation and persisted at least for 5 days (supplemental Figure 10I-J). As expected, the introduction of the *Nfkbiz*-ASO enhanced the expression of *Nfkbiz* in cHSCs compared with SL1- or SL2-targeting ASOs (Figure 7C; supplemental Figure 10K). In contrast, the *Nfkbiz*-ASO did not influence the expression of Reg1 or Reg3, suggesting that the ASO specifically acts on *Nfkbiz* transcripts. Interestingly, *Nfkbiz*-ASO treatment for 5 days mildly but significantly enhanced the expression of myeloid-related genes *Spi1* and *Cebpb*, whereas the treatment reduced *Flt3* expression in cHSCs (Figure 7D). Consistently, cell surface expression of FcγR, a myeloid marker, was slightly augmented in $CD150^{+}CD48^{-}$LSK population by treatment with *Nfkbiz*-ASO (Figure 7E-F). In contrast, the *Nfkbiz*-ASO did not alter the expression of HSC-related genes including *Hlf*, *Cd34*, and *Hoxb5*

(Figure 7D) or the frequency of LSK population (supplemental Figure 10L-M). Whereas *Nfkbiz*-ASO treatment alone slightly induced myeloid differentiation, simultaneous treatment with TNF or IL-1β drastically promoted myeloid differentiation of cultured HSCs (Figure 7G-H). Interestingly, TNF or IL-1β synergized with *Nfkbiz*-ASO and dramatically enhanced FcγR expression in $CD150^{+}CD48^{-}$LSK population of cHSCs (Figure 7E-F). Taken together, the *Nfkbiz*-ASO is potent to induce myeloid-lineage priming in HSCs by enhancing the expression of Nfkbiz.

## Discussion

In the present study, we discovered the Reg1/Reg3-*Nfkbiz* axis acts as the novel regulatory mechanism governing lineage bias in HSPCs, identifying it as a promising target for manipulating hematopoiesis (Figure 7I). It was demonstrated that epigenetic regulation is critical for the lineage specification of HSPCs, and that it is difficult to separate these features of stem cells by known epigenetic factors.[40-43] In this regard, we believe that Reg1 and Reg3 are novel cellular factors to be identified that determine myeloid-lymphoid cell fate decision by controlling HSPCs.

Despite the multiple functions of *Nfkbiz* in various mature immune cells,[32,44-46] its role in HSCs has not yet been discussed. The IκB-ζ protein, encoded by the *Nfkbiz* gene, interacts with NF-κBp50 to reinforce NF-κB activation,[32] and also participates in chromatin remodeling under inflammatory conditions.[44,46] NF-κB has been shown to be involved in emergency myelopoiesis by TNF,[16] and the cooperation between NF-κBp50 and C/EBPα in the granulocytic progenitors for promoting myelopoiesis has been demonstrated.[47] Therefore, *Nfkbiz* expressed by the suppression of Reg1/Reg3 may initiate the myeloid program in cooperation with the NF-κB and/or by recruiting the chromatin remodelers to induce epigenetic changes.

The Reg1/Reg3-*Nfkbiz* regulatory axis is a novel therapeutic target to manipulate myeloid- and lymphoid-biased outputs in hematopoiesis. We found that an ASO disrupting SL structures in *Nfkbiz* 3' UTR is potent to increase *Nfkbiz* expression and induce myeloid-biased lineage priming in HSCs. Given that this ASO specifically targets *Nfkbiz* expression, this strategy might be beneficial compared to the treatment with cytokines/TLR ligands, which can induce broad responses. Indeed, the SL structures targeted by Reg1 and Reg3 are conserved in human *NFKBIZ*. Nevertheless, further studies are required to optimize the sequences and nucleic acids modification as well as drug delivery to improve the efficacy of the therapeutic potential.

In summary, we demonstrate here that Reg1 and Reg3 act as a molecular

switch to control lineage biases in HSPCs by shaping transcriptional lineage priming. These two RNases control multipotent cell lineage choice by targeting *Nfkbiz* for degradation. Nfkbiz acts as a key regulator to promote myeloid-lineage commitment. Our findings provide insights into how HSC lineage priming is regulated.

**Acknowledgements**

We thank H. Miyachi, S. Kitano, R. Takeda, and S. Nagai for animal technical service; T. Maruyama for providing *Nfkbiz* flox mice; Y. Agata for plasmid construction of retroviral expression of human *Id3*, S. Yamazaki for Soluplus, T. Nagasawa, N. Chevrier, and all members of the Takeuchi laboratory for insights and suggestions. Flow cytometric analysis and cell sorting using LSRFortessa (BD) and AriaIII (BD) were performed at the Medical Research Support Center, Graduate School of Medicine, Kyoto University, which was supported by Platform Project for Supporting Drug Discovery and Life Science Research (Basis for Supporting Innovative Drug Discovery and Life Science Research (BINDS)) from AMED (Grant Number JP20am0101092). Figures were created using BioRender.com.

This study was supported by Japan Society for the Promotion of Science (JSPS) KAKENHI [18H05278, 23H00402] to O.T. and [18K15185] to T.U. and Core-to-Core Program to O.T. and Grant-in-Aid for Scientific Research on Innovative Areas 'Genome Science' [221S0002, 16H06279] to T.M. This study was also supported by Japan Agency for Medical Research and Development (AMED) [JP20gm4010002, JP21ae0121030, 23ama221327h0001] to O.T. and the Cooperative Research Program (Joint Usage/Research Center program) of Institute for Frontier Life and Medical Sciences, Kyoto University to O.T. and a Grant-in-Aid for Transformative Research Areas (A) "Material Symbiosis" (Grant 20H05874 to T.U.) and ISHIZUE 2017 of Kyoto University Research Development Program to T.U., an Office of Directors' Research Grant provided by the Institute for Frontier Life and Medical Sciences to A.V., and the Fujiwara Memorial Foundation to T.U.

**Authorship Contributions**

T.U. and O.T. were in charge of experimental designs, analyses, interpretation of data and drafting of the manuscript; S.Y., D.O., K.T., and M.M. participated in the

acquisition, analysis and interpretation of data; A.J., A.G., and I.A. handled scRNA-seq samples and performed analyses on scRNA-seq data. A.V. and K.T. performed analysis of scRNA-seq and scATAC-seq data; Y.M. and M.L. performed HITS-CLIP of Regnase-3; H.K. analyzed HITS-CLIP of Regnase-1 and Regnase-3; H.W. and G.K. contributed to genetic engineering to generate multiple mouse lines; T.T. performed histological examination; T.I. and R.Y. contributed to *in vitro* culture of multipotent progenitors and HSCs, respectively; D.M.S. carried out structural modeling; T.M., M.M., R.Y., H.R.R., and H.K. provided critical discussions and suggestions; O.T. supervised the overall study.

Disclosure of Conflicts of Interest: The authors declare that they have no financial conflict of interest.

## REFERENCES

1. Haas S, Trumpp A, Milsom MD. Causes and Consequences of Hematopoietic Stem Cell Heterogeneity. *Cell Stem Cell*. 2018;22(5):627-638.

2. Hofer T, Rodewald HR. Differentiation-based model of hematopoietic stem cell functions and lineage pathways. *Blood*. 2018;132(11):1106-1113.

3. Olson OC, Kang YA, Passegue E. Normal Hematopoiesis Is a Balancing Act of Self-Renewal and Regeneration. *Cold Spring Harb Perspect Med*. 2020;10(12).

4. Pina C, Fugazza C, Tipping AJ, et al. Inferring rules of lineage commitment in haematopoiesis. *Nat Cell Biol*. 2012;14(3):287-294.

5. Macaulay IC, Svensson V, Labalette C, et al. Single-Cell RNA-Sequencing Reveals a Continuous Spectrum of Differentiation in Hematopoietic Cells. *Cell Rep*. 2016;14(4):966-977.

6. Nestorowa S, Hamey FK, Pijuan Sala B, et al. A single-cell resolution map of mouse hematopoietic stem and progenitor cell differentiation. *Blood*. 2016;128(8):e20-31.

7. Velten L, Haas SF, Raffel S, et al. Human haematopoietic stem cell lineage commitment is a continuous process. *Nat Cell Biol*. 2017;19(4):271-281.

8. Olsson A, Venkatasubramanian M, Chaudhri VK, et al. Single-cell analysis of mixed-lineage states leading to a binary cell fate choice. *Nature*. 2016;537(7622):698-702.

9. Paul F, Arkin Y, Giladi A, et al. Transcriptional Heterogeneity and Lineage Commitment in Myeloid Progenitors. *Cell*. 2016;164(1-2):325.

10. Hirai H, Zhang P, Dayaram T, et al. C/EBPbeta is required for 'emergency' granulopoiesis. *Nat Immunol*. 2006;7(7):732-739.

11. King KY, Goodell MA. Inflammatory modulation of HSCs: viewing the HSC as a foundation for the immune response. *Nat Rev Immunol*. 2011;11(10):685-692.

12. Mossadegh-Keller N, Sarrazin S, Kandalla PK, et al. M-CSF instructs myeloid lineage fate in single haematopoietic stem cells. *Nature*. 2013;497(7448):239-243.

13. Manz MG, Boettcher S. Emergency granulopoiesis. *Nat Rev Immunol*. 2014;14(5):302-314.

14. Pietras EM, Mirantes-Barbeito C, Fong S, et al. Chronic interleukin-1 exposure drives haematopoietic stem cells towards precocious myeloid differentiation at the expense of self-renewal. *Nat Cell Biol*. 2016;18(6):607-618.

15. Chavakis T, Mitroulis I, Hajishengallis G. Hematopoietic progenitor cells as integrative hubs for adaptation to and fine-tuning of inflammation. *Nat Immunol*. 2019;20(7):802-811.

16. Yamashita M, Passegue E. TNF-alpha Coordinates Hematopoietic Stem Cell Survival and Myeloid Regeneration. *Cell Stem Cell*. 2019;25(3):357-372 e357.

17. Collins A, Mitchell CA, Passegue E. Inflammatory signaling regulates hematopoietic stem and progenitor cell development and homeostasis. *J Exp Med*. 2021;218(7).

18. Beerman I, Bock C, Garrison BS, et al. Proliferation-dependent alterations of the DNA methylation landscape underlie hematopoietic stem cell aging. *Cell Stem Cell*. 2013;12(4):413-425.

19. Cullen SM, Mayle A, Rossi L, Goodell MA. Hematopoietic stem cell development: an epigenetic journey. *Curr Top Dev Biol*. 2014;107:39-75.

20. Sun D, Luo M, Jeong M, et al. Epigenomic profiling of young and aged HSCs reveals concerted changes during aging that reinforce self-renewal. *Cell Stem Cell*. 2014;14(5):673-688.

21. Uehata T, Takeuchi O. Post-transcriptional regulation of immunological responses by Regnase-1-related RNases. *Int Immunol*. 2021;33(12):859-865.

22. Mino T, Iwai N, Endo M, et al. Translation-dependent unwinding of stem-loops by UPF1 licenses Regnase-1 to degrade inflammatory mRNAs. *Nucleic Acids Res*. 2019;47(16):8838-8859.

23. Mino T, Murakawa Y, Fukao A, et al. Regnase-1 and Roquin Regulate a Common Element in Inflammatory mRNAs by Spatiotemporally Distinct Mechanisms. *Cell*. 2015;161(5):1058-1073.

24. Matsushita K, Takeuchi O, Standley DM, et al. Zc3h12a is an RNase essential for controlling immune responses by regulating mRNA decay. *Nature*. 2009;458(7242):1185-1190.

25. Uehata T, Iwasaki H, Vandenbon A, et al. Malt1-induced cleavage of regnase-1 in CD4(+) helper T cells regulates immune activation. *Cell*. 2013;153(5):1036-1049.

26. Giladi A, Paul F, Herzog Y, et al. Single-cell characterization of haematopoietic progenitors and their trajectories in homeostasis and perturbed haematopoiesis. *Nat Cell Biol*. 2018;20(7):836-846.

27. Baran Y, Bercovich A, Sebe-Pedros A, et al. MetaCell: analysis of single-cell RNA-seq data using K-nn graph partitions. *Genome Biol*. 2019;20(1):206.

28. Jacobsen SEW, Nerlov C. Haematopoiesis in the era of advanced single-cell technologies. *Nat Cell Biol*. 2019;21(1):2-8.

29. Iancu-Rubin C, Gajzer D, Tripodi J, et al. Down-regulation of stathmin expression is required for megakaryocyte maturation and platelet production. *Blood*. 2011;117(17):4580-4589.

30. Klein F, Roux J, Cvijetic G, et al. Dntt expression reveals developmental hierarchy and lineage specification of hematopoietic progenitors. *Nat Immunol*. 2022;23(4):505-517.

31. Ikawa T, Masuda K, Huijskens M, et al. Induced Developmental Arrest of Early Hematopoietic Progenitors Leads to the Generation of Leukocyte Stem Cells. *Stem Cell Reports*. 2015;5(5):716-727.

32. Yamamoto M, Yamazaki S, Uematsu S, et al. Regulation of Toll/IL-1-receptor-mediated gene expression by the inducible nuclear protein IkappaBzeta. *Nature*. 2004;430(6996):218-222.

33. Kayama H, Ramirez-Carrozzi VR, Yamamoto M, et al. Class-specific regulation of pro-inflammatory genes by MyD88 pathways and IkappaBzeta. *J Biol Chem*. 2008;283(18):12468-12477.

34. Pietras EM, Reynaud D, Kang YA, et al. Functionally Distinct Subsets of Lineage-Biased Multipotent Progenitors Control Blood Production in Normal and Regenerative Conditions. *Cell Stem Cell*. 2015;17(1):35-46.

35. Sommerkamp P, Romero-Mulero MC, Narr A, et al. Mouse multipotent progenitor 5 cells are located at the interphase between hematopoietic stem and progenitor cells. *Blood*. 2021;137(23):3218-3224.

36. Ranzoni AM, Tangherloni A, Berest I, et al. Integrative Single-Cell RNA-Seq and ATAC-Seq Analysis of Human Developmental Hematopoiesis. *Cell Stem Cell*. 2021;28(3):472-487 e477.

37. Lorenz R, Bernhart SH, Honer Zu Siederdissen C, et al. ViennaRNA Package 2.0. *Algorithms Mol Biol*. 2011;6:26.

38. Tse KM, Vandenbon A, Cui X, et al. Enhancement of Regnase-1 expression with stem loop-targeting antisense oligonucleotides alleviates inflammatory diseases. *Sci Transl Med*. 2022;14(644):eabo2137.

39. Wilkinson AC, Ishida R, Kikuchi M, et al. Long-term ex vivo haematopoietic-stem-cell expansion allows nonconditioned transplantation. *Nature*. 2019;571(7763):117-121.

40. Ko M, Bandukwala HS, An J, et al. Ten-Eleven-Translocation 2 (TET2) negatively regulates homeostasis and differentiation of hematopoietic stem cells in mice. *Proc Natl Acad Sci U S A*. 2011;108(35):14566-14571.

41. Challen GA, Sun D, Mayle A, et al. Dnmt3a and Dnmt3b have overlapping and distinct functions in hematopoietic stem cells. *Cell Stem Cell*. 2014;15(3):350-364.

42. Lara-Astiaso D, Weiner A, Lorenzo-Vivas E, et al. Immunogenetics. Chromatin state dynamics during blood formation. *Science*. 2014;345(6199):943-949.

43. Avgustinova A, Benitah SA. Epigenetic control of adult stem cell function. *Nat Rev Mol Cell Biol*. 2016;17(10):643-658.

44. Miyake T, Satoh T, Kato H, et al. IkappaBzeta is essential for natural killer cell

activation in response to IL-12 and IL-18. *Proc Natl Acad Sci U S A*. 2010;107(41):17680-17685.

45. Okamoto K, Iwai Y, Oh-Hora M, et al. IkappaBzeta regulates T(H)17 development by cooperating with ROR nuclear receptors. *Nature*. 2010;464(7293):1381-1385.

46. Tartey S, Matsushita K, Vandenbon A, et al. Akirin2 is critical for inducing inflammatory genes by bridging IkappaB-zeta and the SWI/SNF complex. *EMBO J*. 2014;33(20):2332-2348.

47. Wang D, Paz-Priel I, Friedman AD. NF-kappa B p50 regulates C/EBP alpha expression and inflammatory cytokine-induced neutrophil production. *J Immunol*. 2009;182(9):5757-5762.

**Figure Legends**

**Figure 1. Reg1 and Reg3 are essential for early-stage lymphopoiesis in a cell-intrinsic manner.** (A-F) Competitive FL transplantation. (A) Experimental workflow of competitive transplantation using fetal liver (FL) cells (E15.5). (B-C) Relative frequencies and cell numbers of donor immune cells in the peripheral blood. (B) Each dot represents the ratio of the percentage of CD45.2 in each population to the percentage of CD45.2 in SLAM$^{+}$ Lin$^{-}$Sca1$^{+}$Kit$^{+}$ (LSK) from recipient mice. Donor B cells, T cells, and myeloid cells were defined as CD45.2$^{+}$ B220$^{+}$CD19$^{+}$ cells, CD4/8$^{+}$TCRβ$^{+}$ cells, and CD11b$^{+}$ cells, respectively. (D) Representative flow cytometric plots of CD45.1 and CD45.2 expression gated on CD150$^{+}$ LSK, LMPP (Flt3$^{hi}$LSK), CLP (Ly6D$^{-}$Flt3$^{+}$IL-7Rα$^{+}$Sca1$^{dull}$Kit$^{dull}$), and BLP (Ly6D$^{+}$Flt3$^{+}$IL-7Rα$^{+}$Sca1$^{dull}$Kit$^{dull}$). Numbers in plots indicate the percentage of CD45.1$^{+}$ or CD45.2$^{+}$ cells. (E-F) Relative frequencies of each population in the BM. Each dot represents the ratio of the percentage of CD45.2 in each population to the percentage of CD45.2 in CD150$^{+}$ LSK from recipient mice. (G-H) *in vivo* BrdU incorporation and Annexin V staining in CD150$^{+}$ LSK, CD150$^{-}$ LSK, Flt3$^{+}$ MPP, CLP, CMP, GMP, and MEP in the BM of mice competitively transplanted with FL cells, as in (A). (E,F) Data are a composite of three independent experiments. (G,H) Data are representative from three independent experiments. Data are presented as mean ± SD (B,C,E-H). Statistical significance was calculated by unpaired two-tailed Student's *t*-test (B,C,E-H). ns, not significant.

**Figure 2. Reg1 and Reg3 control lineage biases within HSPCs.** (A) Schematic representation of experimental strategy for single-cell sorting. (B) Gating strategy for WT and *Reg1*$^{-/-}$*Reg3*$^{-/-}$ (DKO) LSK cells sorted from the identical mouse receiving WT (CD45.1) and DKO (CD45.2) FL cells. (C) A two-dimensional projection of 2,241 single cells sorted from WT (CD45.1) LSK and 2,242 single cells from DKO (CD45.2)

LSK onto the reference model. Cells are colored according to assignment to reference model meta-cells (see Methods). (D) Difference in meta-cell abundance between single cells sorted from DKO and WT mice. Each circle represents a reference meta-cell. Circle color represents $\log_2$ (fold change) in meta-cell abundance between the two genetic backgrounds. **e**, Cell type distribution of single cells sorted from WT and DKO mice. *$p < 0.05$; **$p < 0.001$; ***$p < 0.00001$. (F) Differential gene expression between pooled cells from DKO cells compared to WT cells. Gold dots indicate differentially expressed genes (FDR corrected $p < 0.001$ under Chi-square test) with fold change > 2. Diagonal lines show $\log_2$ (fold change) = –1 or 1. Values represent $\log_2$ size-normalized expression. (G) Total expression of specific genes in different genetic backgrounds. Values represent size-normalized total transcripts per 100 cells. Colors represent relative contribution from the different hematopoietic core subsets. (H) Luciferase activity was assessed by using pGL3 plasmids containing 3'UTR of *Nfkbiz* and *Ehd3*, together with mock or plasmids for wild-type (WT) or nuclease-dead (ND) mutant for Reg1 and Reg3 (n = 3 each). Data are representative of at least three independent experiments. (I) mRNA stability of *Nfkbiz* and *Ehd3* in $Lin^-$ cells from control and $DKO^{CreERT2}$ mice. Cells were stimulated with IL-1β for 2 hours, followed by addition of actinomycin D (ActD). The remaining transcripts relative to the 0 h time point were measured by quantitative RT-PCR. Data are representative of two independent experiments (H, I). Data are presented as mean ± SD (H) or ± SEM (I). Statistical significance was calculated by two-tailed Fisher's exact test (E), one-way ANOVA with Holm-Sidak multiple comparisons test (H), or unpaired two-tailed Student's *t*-test (I). ns, not significant.

**Figure 3. Nfkbiz is a direct target gene for Reg1 and Reg3 that is potent to promote myelopoiesis.** (A) Schematic representation for B cell differentiation of multipotent progenitor ($MPP^{hId3\text{-}ERT2}$) cells retrovirally transduced with MSCV-Thy1.1 vector. Cells

were then cultured under B cell-differentiation condition. (B-C) *In vitro* B cell differentiation in MPP$^{hId3\text{-}ERT2}$ cells retrovirally overexpressing Nfkbiz and Ehd3 as well as myeloid lineage TFs. At day 7, cells were analyzed by flow cytometry. Flow cytometry plots of CD19 and CD11b after gated on Thy1.1$^{+}$ cells (B) and percentages of CD19$^{+}$ and CD11b$^{+}$ Thy1.1$^{+}$ cells (C) were shown (n = 6 each). (D) Numbers of CD19$^{+}$CD11b$^{-}$ and CD19$^{-}$CD11b$^{+}$ cells in tetO-*cre*-*Reg1*$^{fl/fl}$*Reg3*$^{-/-}$ MPP$^{hId3\text{-}ERT2}$ cells cultured under B cell-differentiating condition in the presence or absence of DOX at day 6 (n = 6 each). (E-F) Quantitative RT-PCR (E) and immunoblot analysis (F) of *Nfkbiz* in tetO-*cre*-*Reg1*$^{fl/fl}$*Reg3*$^{-/-}$ MPP$^{hId3\text{-}ERT2}$ cells at the indicated time points after DOX treatment (n = 3 each in E). Cells were cultured under stem-cell condition for the indicated time. (G) DOX-inducible overexpression of FLAG-tagged Reg1 (D141N) or Reg3 (D271N) in tetO-*cre*-*Reg1*$^{fl/fl}$*Reg3*$^{-/-}$ MPP$^{hId3\text{-}ERT2}$ cells. (H) RIP-qPCR analysis of a set of genes from lysates of tetO-*cre*-*Reg1*$^{fl/fl}$*Reg3*$^{-/-}$ MPP$^{hId3\text{-}ERT2}$ cells expressing FLAG-tagged Reg1 or Reg3 as in (G) (n = 4 each). Data are representative of two (B-D, G-H) or at least three (E-F) independent experiments. Data are presented as mean ± SD (C-E, H). Statistical significance was calculated by one-way ANOVA with Holm-Sidak multiple comparisons test (C, E, H) or unpaired two-tailed Student's *t*-test (D). ns, not significant.

**Figure 4. The Reg1/Reg3-*Nfkbiz* axis controls lymphoid-myeloid fate decision.** (A-C) Representative flow cytometry plots (A), frequencies (B) and cell numbers (C) of HSPC subpopulations in mice of the indicated genotypes at day14 after tamoxifen treatment. *Ctrl*, CreERT2$^{+}$*Reg1*$^{fl/+}$*Reg3*$^{+/+}$*Nfkbiz*$^{fl/+}$; *Nfkbiz*$^{CreERT2}$, CreERT2$^{+}$*Reg1*$^{fl/+}$*Reg3*$^{+/+}$*Nfkbiz*$^{fl/fl}$; *DKO*$^{CreERT2}$, CreERT2$^{+}$*Reg1*$^{fl/fl}$*Reg3*$^{-/-}$*Nfkbiz*$^{+/+}$; *TKO*$^{CreERT2}$, CreERT2$^{+}$*Reg1*$^{fl/fl}$*Reg3*$^{-/-}$*Nfkbiz*$^{fl/fl}$ (n = 4 each). Asterisks represents *P*-value (*$p < 0.05$; **$p < 0.01$; ****$p < 0.0001$). (D-F) Representative flow cytometry plots (D), and frequency (E) and cell number (F) of B cells in the indicated mice ($n = 4$ each). (G-I)

Representative flow cytometry plots (G), and frequencies (H) and cell numbers (I) of myeloid cells in the indicated mice (n = 4 each). (J-L) *In vitro* B cell differentiation using $Lin^{-}Kit^{+}IL\text{-}7R\alpha^{+}$ FL cells derived from the indicated genotypes. Progenitor cells were differentiated under B cell-promoting condition in the presence of 4-OHT. *Ctrl*, $CreERT2^{+}Reg1^{fl/+}Reg3^{+/+}Nfkbiz^{fl/+}$; $Nfkbiz^{CreERT2}$, $CreERT2^{+}Reg1^{fl/+}Reg3^{+/+}Nfkbiz^{fl/fl}$; $DKO^{CreERT2}$, $CreERT2^{+}Reg1^{fl/fl}Reg3^{-/-}Nfkbiz^{+/+}$; $TKO^{CreERT2}$, $CreERT2^{+}Reg1^{fl/fl}Reg3^{-/-}Nfkbiz^{fl/fl}$. Representative flow cytometry plots (J), frequency (K) and absolute number (L) of $CD19^{+}B220^{+}$ cells are shown. n = 6. Data are a composite of two independent experiments (A-I) or a representative of two independent experiments (J-L). Data are presented as mean ± SD (C, E-F, H-I, K-L). Statistical significance was calculated by one-way ANOVA with Holm-Sidak multiple comparisons test. ns, not significant.

**Figure 5. The Reg1/Reg3-*Nfkbiz* axis regulates lineage priming of HSCs/early MPPs via chromatin remodeling.** (A) Schematic representation of scATAC-seq using $Flt3^{-}CD48^{-}$ LSK. In each genotype, samples are pooled from multiple mice to create a single sample for sequencing, as indicated by the number of mice represented. (B) UMAP visualization of all cells obtained from scATAC-seq data. Colors represent the cluster identity. (C) Heatmap showing chromatin accessibility for stemness-related and lineage-associated genes. (D) Cluster distribution of single cells across the indicated genotypes. Colors represent the cluster identity as in (B). (E) A two-dimensional projection of 13859, 10991, 9936, and 6902 single cells from control, $DKO^{CreERT2}$, $Nfkbiz^{CreERT2}$ and $TKO^{CreERT2}$, respectively, onto the UMAP plot (B). (F) Heatmap showing differential chromatin accessibilities of the selected myeloid-related gene loci between control and $DKO^{CreERT2}$ cells in C1-C5. (G-H) Volcano plot showing the comparison of TF motif enrichment between control vs $DKO^{CreERT2}$ in C1-C5 (G) and C6-C8 (H).

**Figure 6. Reg1 and Reg3 recognize the tandem UAU-SL structures present in *Nfkbiz* 3'UTR.** (A) Phosphoimage of SDS-PAGE of radiolabelled Reg3-RNA complexes obtained by immunoprecipitation with anti-FLAG antibody. (B) Pie chart deciphering the distribution of Reg3-binding sites obtained by the intersection of two biological HITS-CLIP replicates. (C-D) SL enrichments in Reg3- and Reg1-bound CLIP tags of 3'UTR compared to 1000 individual sequence permutations. X axis indicates hairpin types where the numbers represent the lengths of stem and loop. Asterisks represent *p*-value. (E-F) Sequence logo representations of the recognition motives for Reg3 and Reg1. Stem and hairpin regions are indicated as S or H in the X axis. (G) Schematic representation of the artificial SL structure and its mutant forms (M1 and M2) in which the SL structure is disrupted. (H) Luciferase activity was assessed by using pGL3-βGlo plasmids containing 3'UTR with SL, M1, M2, and M1+M2 as shown in (G). HeLa cells were transfected with pGL3 plasmids together with expression plasmids for wild-type (WT) Reg1, WT or nuclease-dead (ND) mutant of Reg3 (n = 3 each). (I) Luciferase activity was assessed by using pGL3-βGlo plasmids SL-containing 3'UTR with a set of loop sequences. The loop sequences tested are shown in the top of figures. Transfection was performed as in (H) (n = 3 each). (J) Schematic representation of mouse *Nfkbiz* SL structures targeted by Reg1 and Reg3. M1 and M2 represent mutant sequences that no longer form SL structures. (K) Luciferase activity was assessed by using pGL3-βGlo plasmids containing either WT or mutated SL sequences (M1, M2, or M1+M2) as shown in (J). HeLa cells were transfected with pGL3 plasmids together with expression plasmids for WT or ND mutant of Reg1 and Reg3 (n = 3 each). Data are representative of two to three independent experiments (H-I, K). Data are presented as mean ± SD (H-I, K). Statistical significance was calculated by one-way ANOVA with Holm-Sidak multiple comparisons test (H-I, K). ns, not significant.

**Figure 7. Manipulation of *Nfkbiz* expression by ASO alters HSC lineage priming**

**toward myeloid lineage.** (A) Schematic representation of antisense oligonucleotide (ASO) (shown in red) for Reg1/Reg3-targeting SL structures in mouse *Nfkbiz* 3'UTR. (B) Experimental design for ASO-transduced HSCs. HSCs were electroporated with control oligo or *Nfkbiz*-targeting ASO. Cells were used for subsequent analyses in (C-H). (C-D) qRT-PCR analysis of *Nfkbiz*, *Reg1*, *Reg3*, and HSC/lineage-related genes in cultured HSCs at day 5 after electroporation (n = 5 each). (E-F) Representative flow cytometry plots and frequency of FcγR expression in $CD48^{-}CD150^{+}$ LSK from cultured HSCs stimulated with IL-1β or TNF for 24 hours (n = 3 each). (G-H) Representative flow cytometry plots and frequency of $Fc\gamma R^{+}CD11b^{+}$ cells from cultured HSCs stimulated with IL-1β or TNF for 24 hours (n = 3 each). (I) Model of the Reg1/Reg3-*Nfkbiz* axis in the control of HSC lineage priming. Data are representative of three independent experiments (C-H). Data are presented as mean ± SD (C-D, F, H) Statistical significance was calculated by unpaired two-tailed Student's *t*-test (C-D, F, H). ns, not significant.

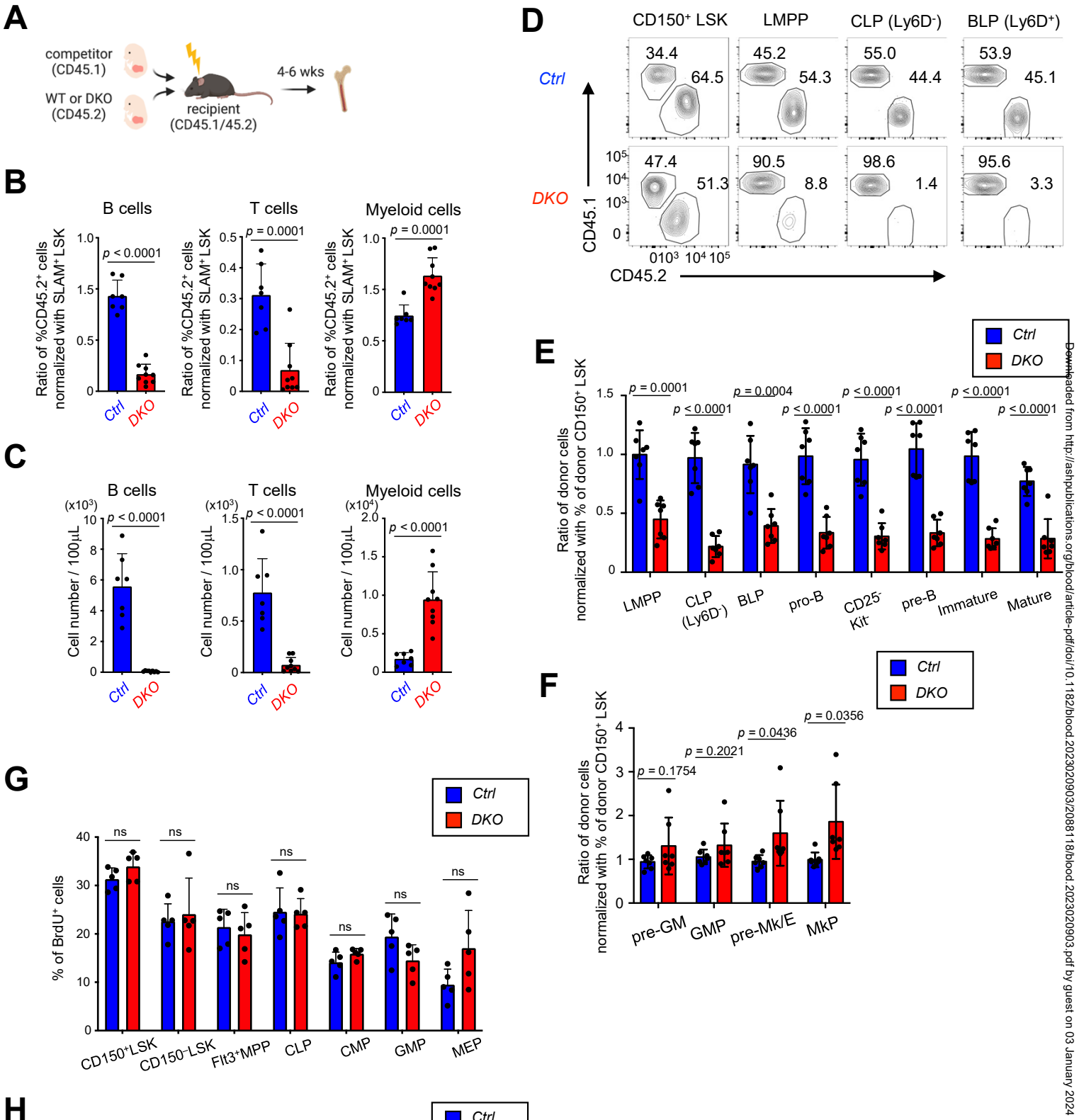




**Figure 1**

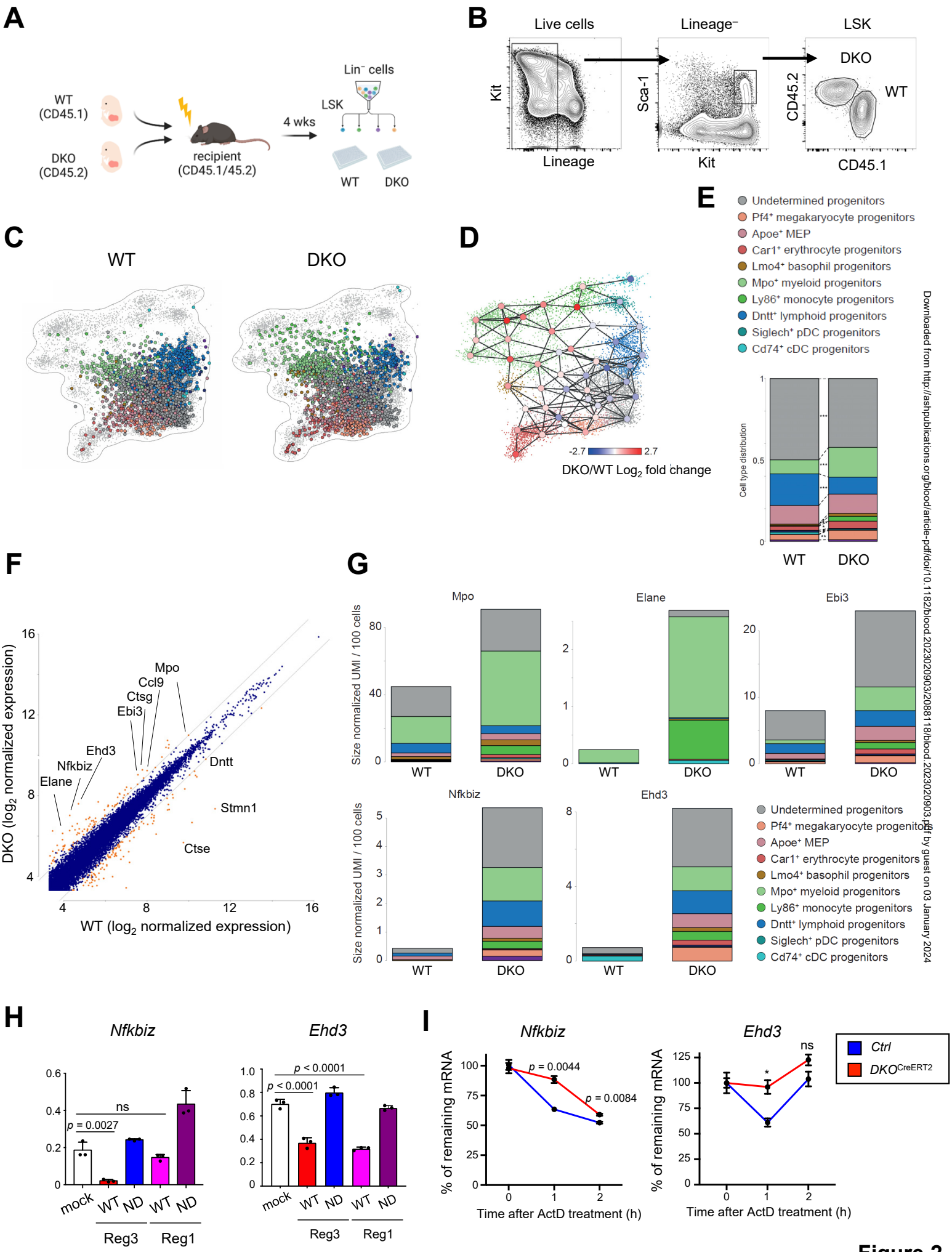




**Figure 2**

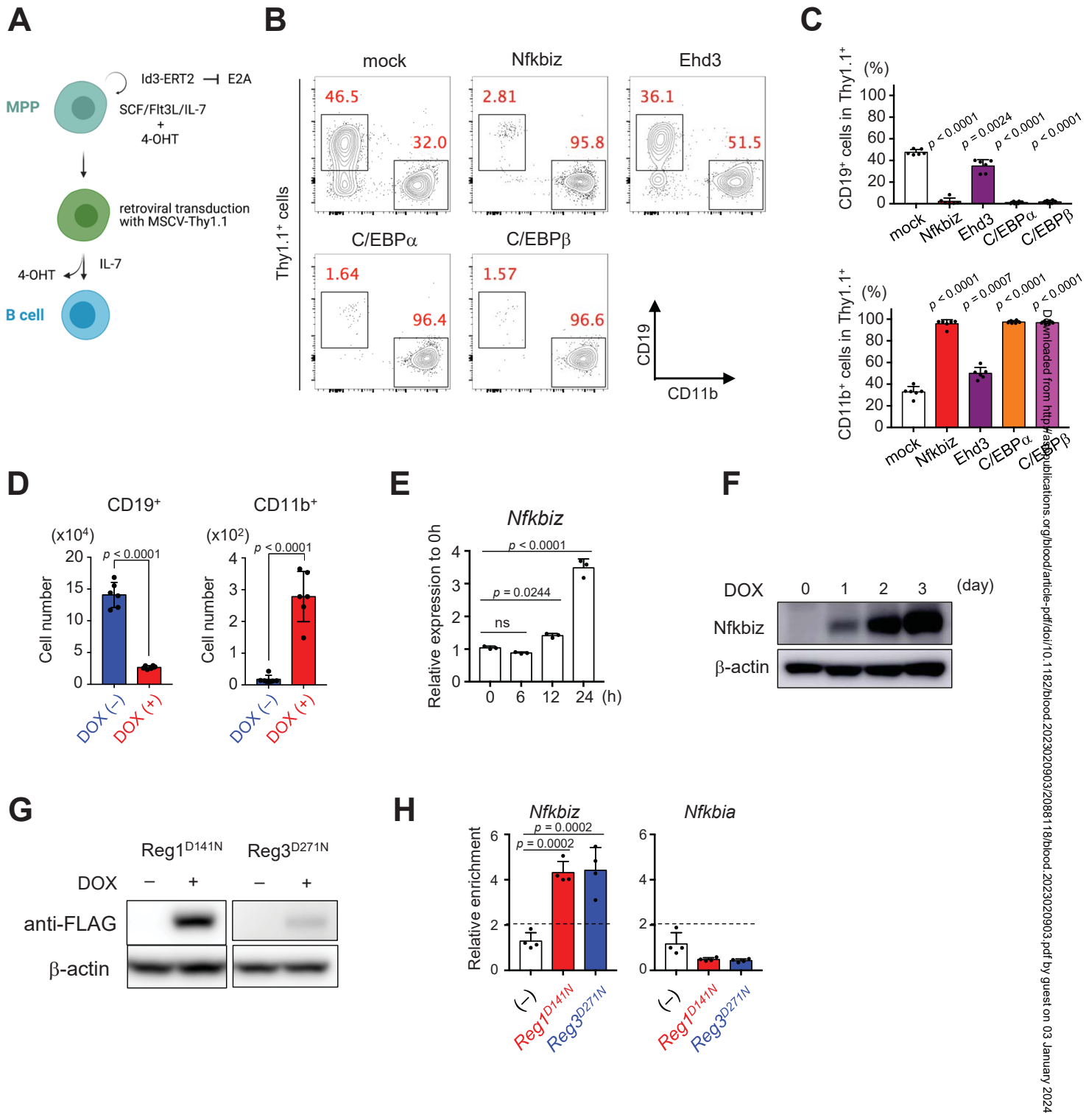




Figure 3

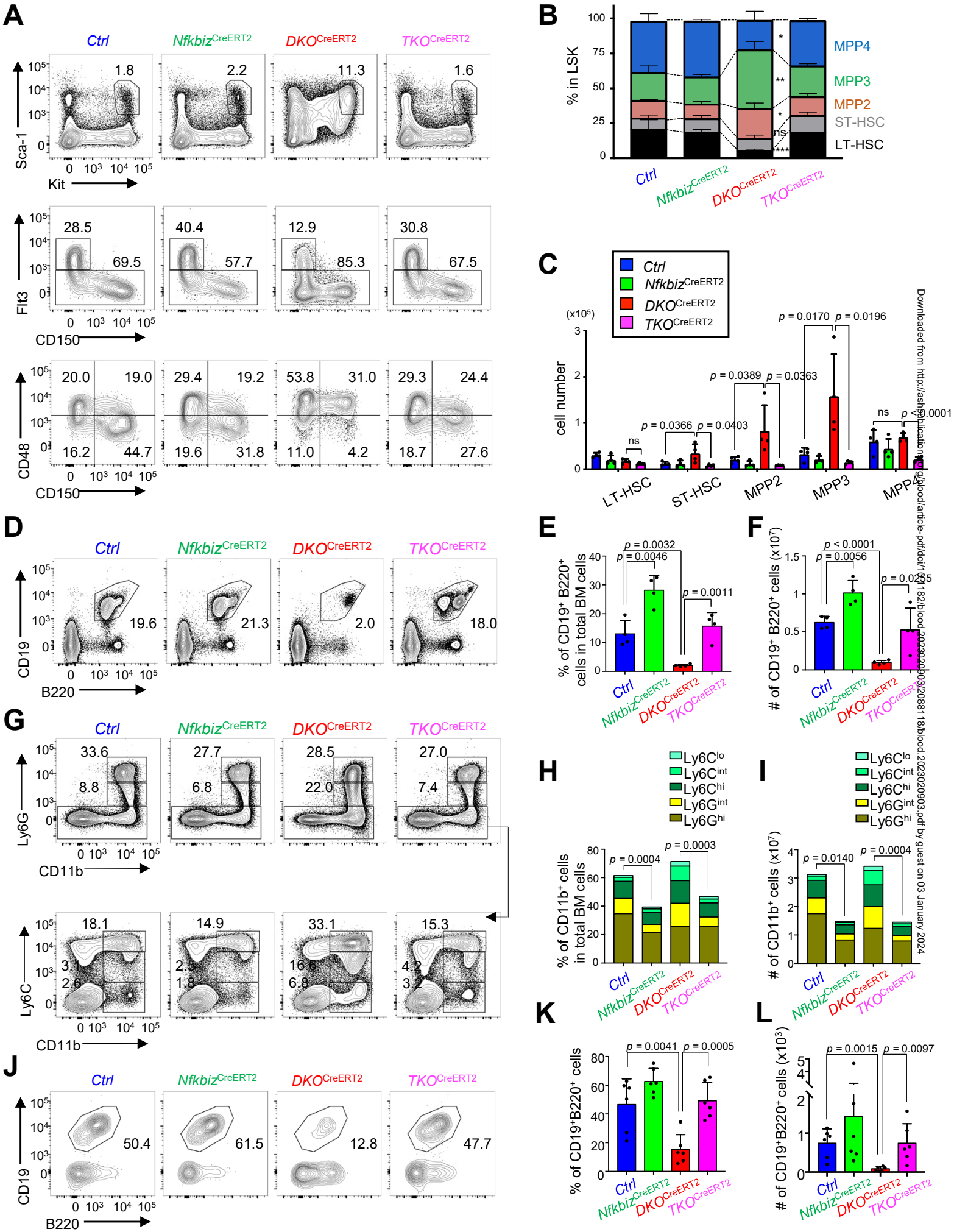




**Figure 4**

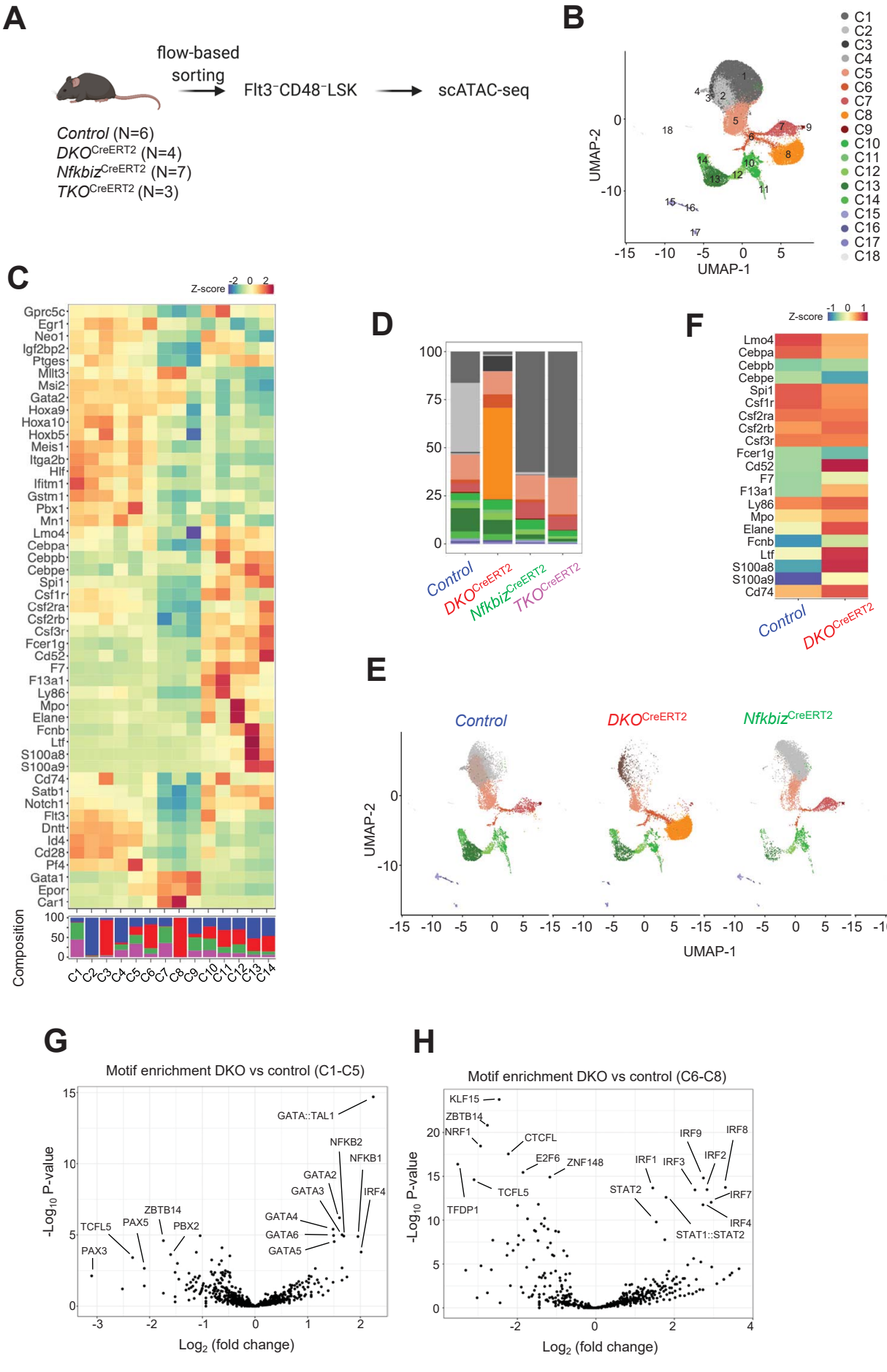




**Figure 5**

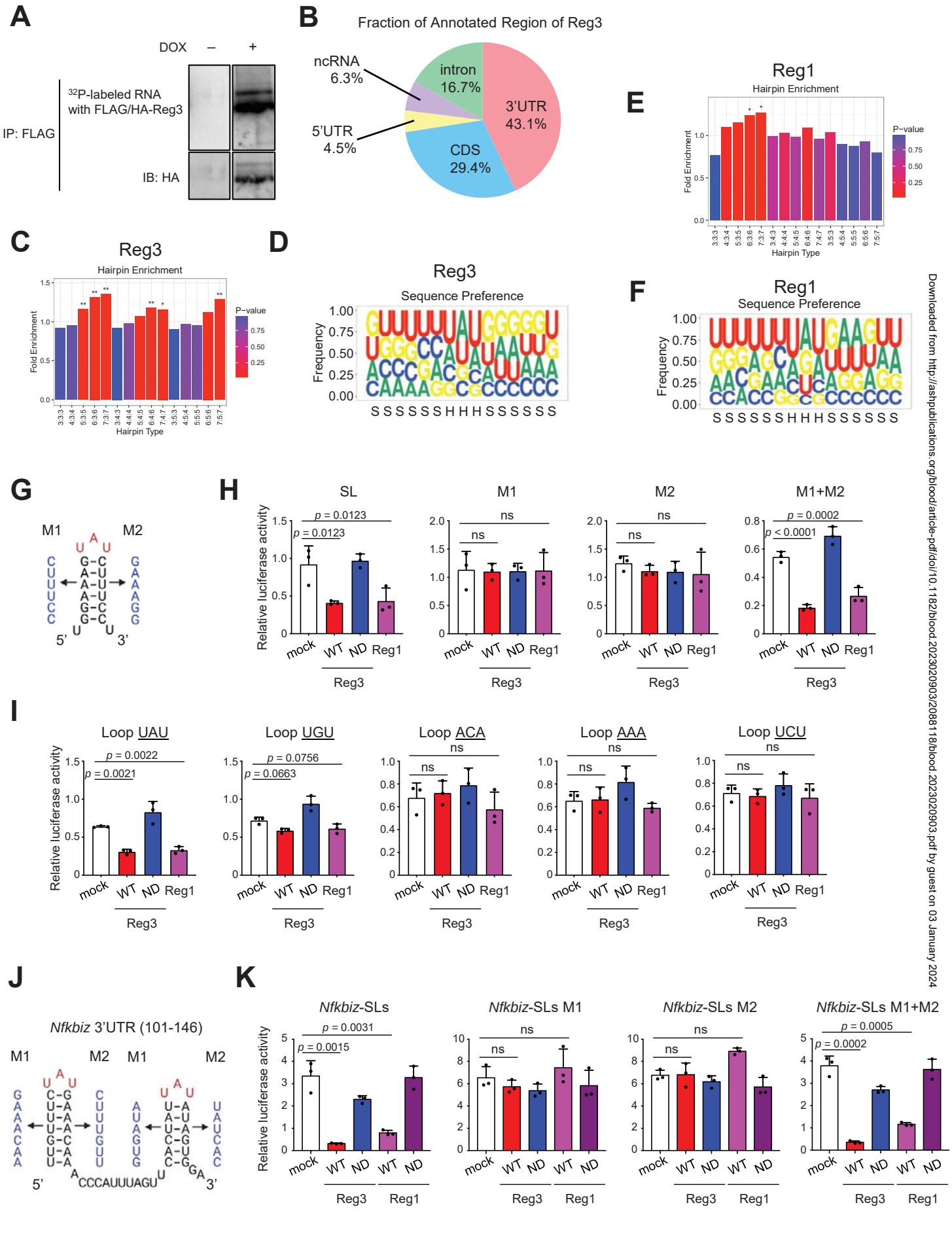




**Figure 6**

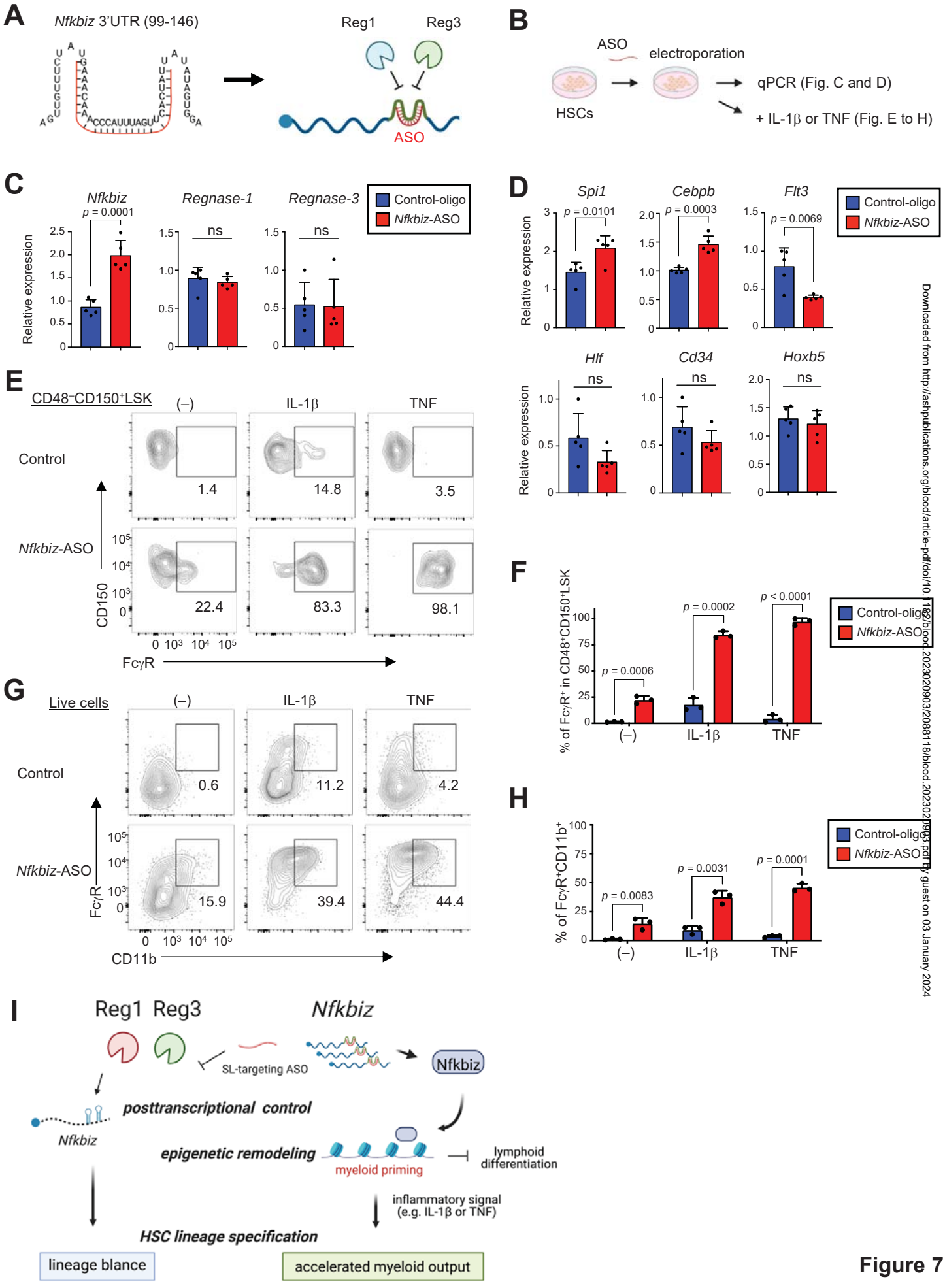


**Figure 7**

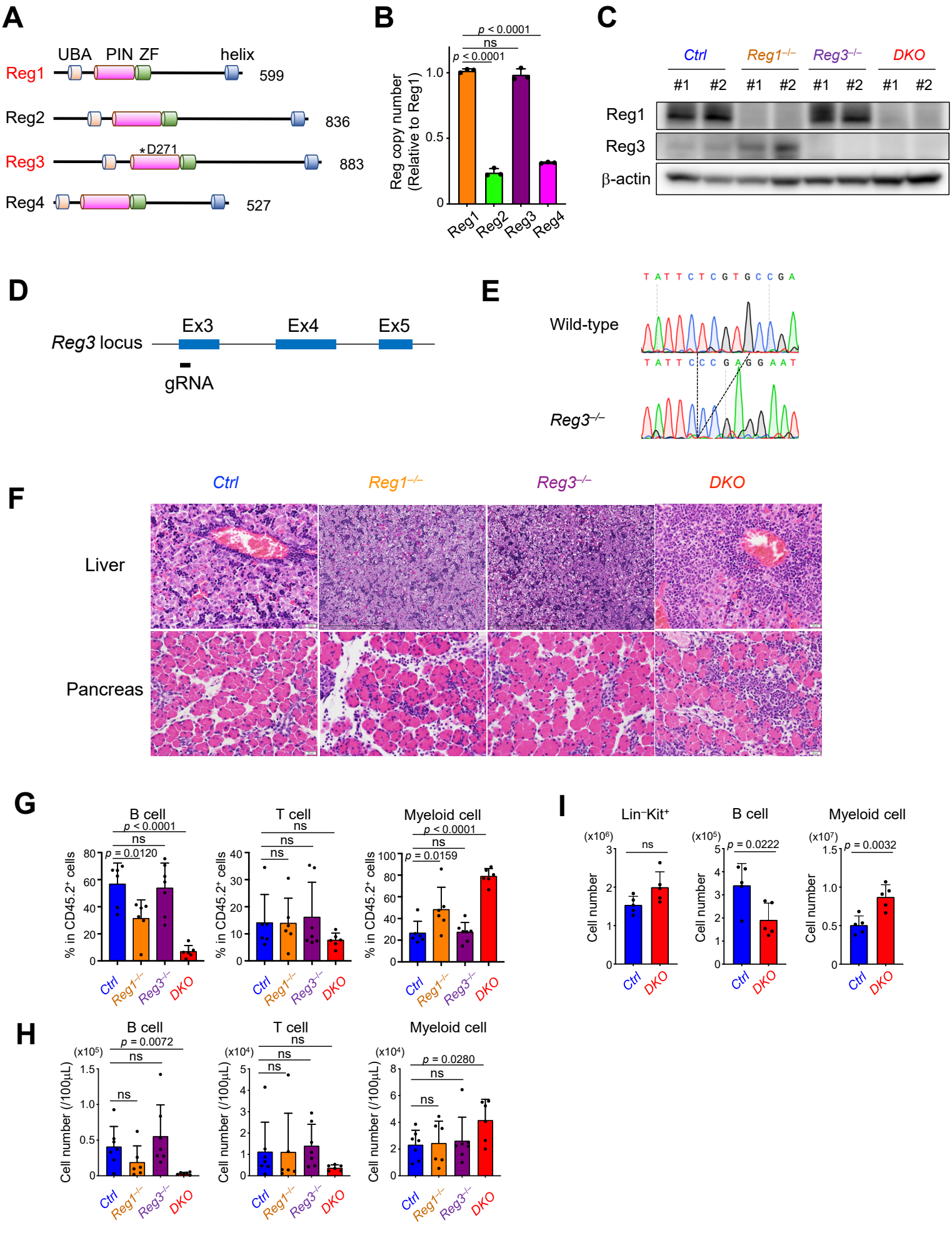
A
UBA
PIN
ZF
helix
Reg1
599
Reg2
836
*D271
Reg3
883
Reg4
527
B
p < 0.0001
ns
p < 0.0001
Reg copy number (Relative to Reg1)
1.0
0.5
0
Reg1
Reg2
Reg3
Reg4
C
Ctrl
Reg1−/−
Reg3−/−
DKO
#1
#2
#1
#2
#1
#2
#1
#2
Reg1
Reg3
β-actin
D
Reg3 locus
Ex3
Ex4
Ex5
gRNA
E
Wild-type
Reg3−/−
F
Ctrl
Reg1−/−
Reg3−/−
DKO
Liver
Pancreas
G
B cell
T cell
Myeloid cell
p < 0.0001
ns
p = 0.0120
p < 0.0001
ns
p = 0.0159
% in CD45.2+ cells
Ctrl
Reg1−/−
Reg3−/−
DKO
I
Lin−Kit+
B cell
Myeloid cell
(x10^6)
(x10^5)
(x10^7)
ns
p = 0.0222
p = 0.0032
Cell number
Ctrl
DKO
H
B cell
T cell
Myeloid cell
(x10^5)
(x10^4)
(x10^4)
p = 0.0072
p = 0.0280
ns
Cell number (/100μL)

**Supplemental Figure 1. Double deficiency of *Reg1* and *Reg3* causes neonatal lethality accompanied by the neutrophil infiltration in the liver and pancreas** (A) Schematic representation of domain structures for Reg family proteins. Asterisk in Reg3 represents the position of amino acid essential for nuclease activity. (B) Relative expression levels of Regnase family genes in bone marrow (BM) lineage-negative ($Lin^-$) cells (n = 3). Copy numbers of Regnase family genes were normalized to Reg1 copy number. (C) Immunoblot analysis of Reg1 and Reg3 in $Lin^-$ cells from mice reconstituted with fetal liver (FL) cells of the indicated genotypes. (D) Schematic representation of strategy for generation of *Reg3*$^{-/-}$ mice by CRISPR-Cas9 system. (E) 5-mer deletion within exon 3 of *Reg3* locus in the mutant allele. (F) H&E staining of liver and pancreas from neonates. (G-H) Percentages and cell numbers of donor B cells ($CD19^+B220^+$), T cells ($CD4/8^+TCR\beta^+$), and myeloid cells ($CD19^-CD11b^+$) in the peripheral blood from FL-transplanted mice (*Ctrl,* n = 6; *Reg1*$^{-/-}$, n = 6; *Reg3*$^{-/-}$, n = 7; *DKO*, n = 6). Mice (CD45.1) reconstituted with FL cells of the indicated genotypes (CD45.2) were analyzed 4-6 weeks post-transplantation, shown in Figure 1A. (I) Cell numbers of $Lin^-Kit^+$ progenitors, $CD19^+B220^+$ cells, and $CD19^-B220^-$ Myeloid markers$^+$ (CD11b/CD11c/Gr-1/DX5) cells in the FL of E15.5 fetuses of the indicated genotypes. (*Ctrl,* n = 5; *DKO*, n = 5). Data are representative of two independent experiments (B, C, G-I). Bar graphs are presented as mean ± SD (G-I). Statistical significance was calculated by one-way ANOVA with Holm-Sidak multiple comparisons test (G, H). Unpaired two-tailed Student's *t*-test (I). ns, not significant.

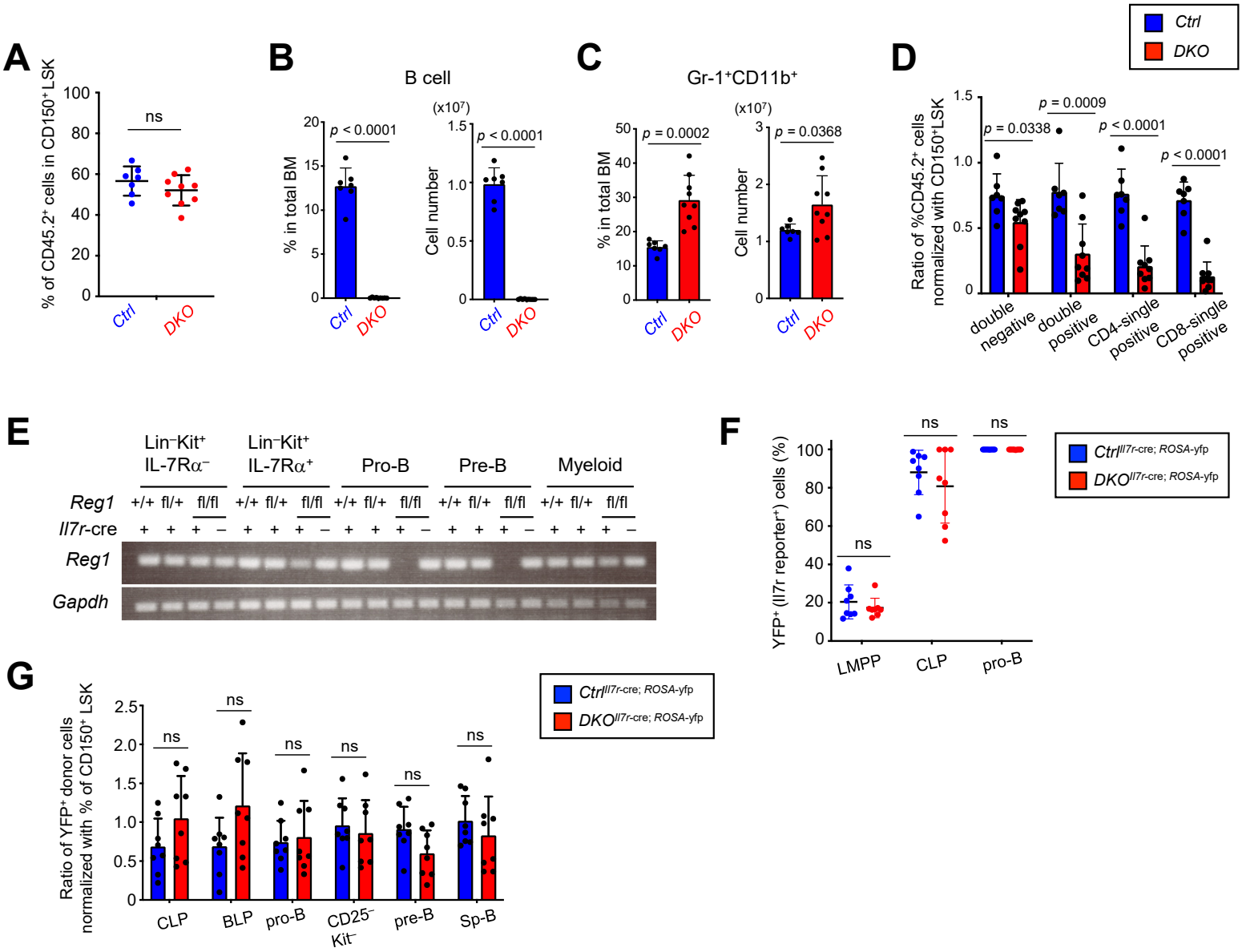


**Supplemental Figure 2. Deletion of *Reg1* and *Reg3* resulted in a profound defect in T/B lymphopoiesis in a cell-intrinsic manner** (A-D) Competitive transplantation of control (*Ctrl*) or *Reg1*$^{-/-}$*Reg3*$^{-/-}$ (*DKO*) FL cells (CD45.2) together with competitors (CD45.1) (*Ctrl*, n = 7; *DKO*, n = 9). (A) Percentages of CD45.2$^{+}$ cells in SLAM$^{+}$LSK population from FL-reconstituted mice. (B-C) Frequencies and cell numbers of CD19$^{+}$ B220$^{+}$ and Gr-1$^{+}$ CD11b$^{+}$ cells in the BM of FL competitively-transplanted mice (D) Thymic development of FL-transplanted mice. Each dot represents the ratio of the percentage of CD45.2 in each population to the percentage of CD45.2 in CD150$^{+}$ LSK from a single recipient mouse. (E) RT-PCR analysis of *Reg1* in FL cells from fetuses of the indicated genotypes. RNA was prepared from Lin$^{-}$Kit$^{+}$IL-7Rα$^{-}$, Lin$^{-}$Kit$^{+}$IL-7Rα$^{+}$, Pro-B, Pre-B, and CD11b$^{+}$ myeloid lineage cells. (F) Percentages of YFP$^{+}$ cells in donor cells (CD45.2) from mice competitively transplanted with FL cells from *Il7r*-cre$^{+}$ROSA$^{yfp/+}$*Reg1*$^{fl/+}$*Reg3*$^{+/-}$ (*Ctrl*$^{Il7r\text{-}cre}$) or *Il7r*-cre$^{+}$ROSA$^{yfp/+}$*Reg1*$^{fl/fl}$*Reg3*$^{-/-}$ (*DKO*$^{Il7r\text{-}cre}$) fetuses (CD45.2) along with *Il7r*-cre$^{+}$ROSA$^{yfp/+}$ fetuses (CD45.1/45.2) (n = 8, each) . (G) B cell development of mice competitively transplanted as in (F). Each dot represents the ratio of the percentage of CD45.2 in YFP$^{+}$ donor cells of each population to the percentage of CD45.2 in CD150$^{+}$ LSK from a single recipient mouse. Data are a composite of three independent experiments. Data are representative of two (E) of three (A-D, F) independent experiments. Data are presented as mean ± SD (A-D, F-G). Statistical significance was calculated by unpaired two-tailed Student's *t*-test.

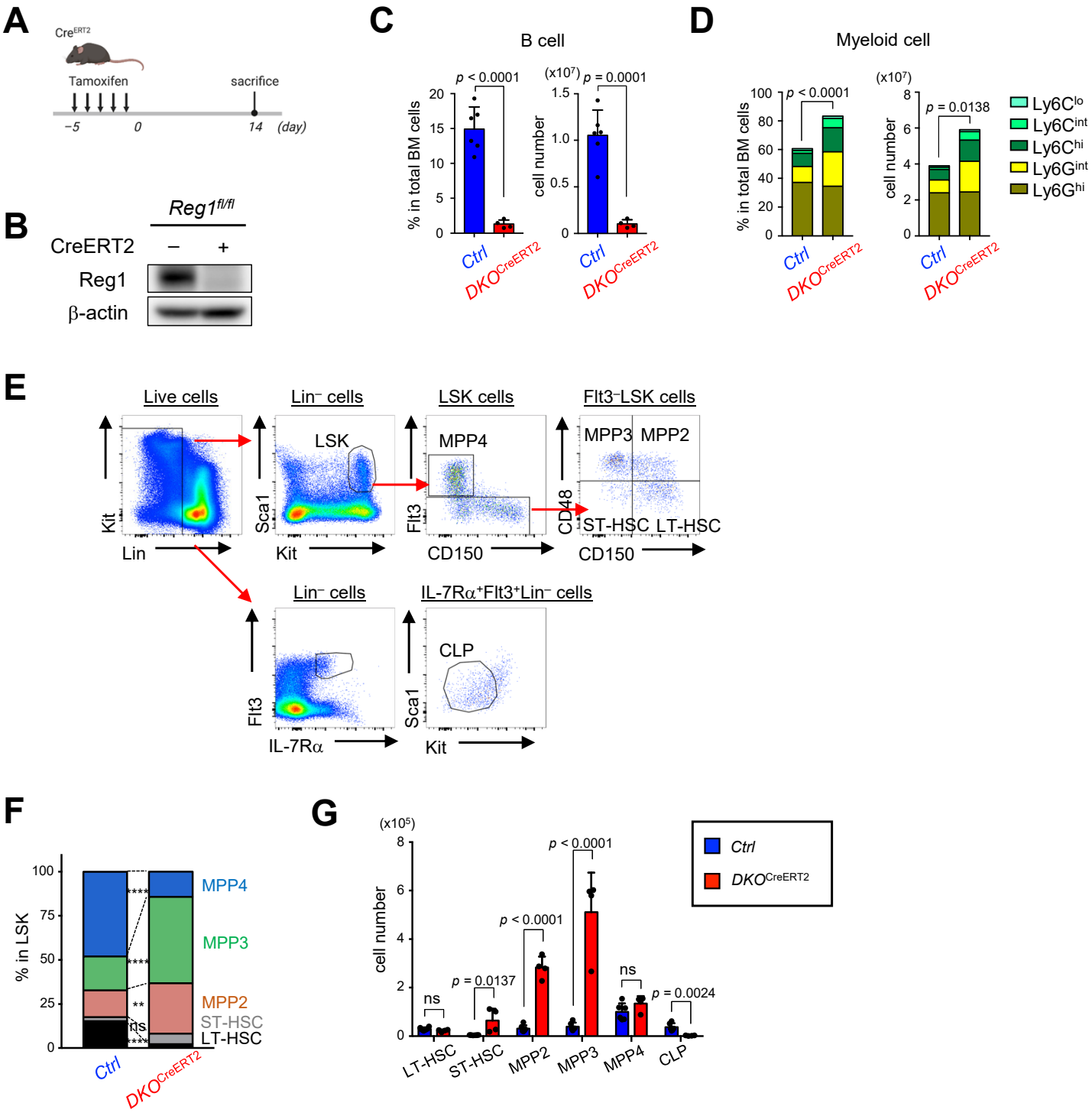


**Supplemental Figure 3. Inducible deletion of *Reg1* in the absence of *Reg3* results in altered hematopoiesis favoring myeloid lineages**

(A) Experimental design for *in vivo* tamoxifen injection. (B) Immunoblot analysis of Reg1 in Lin$^-$ BM cells from CreERT2$^-$ and CreERT2$^+$*Reg1*$^{fl/fl}$ mice. BM cells were harvested from mice at day 3 after tamoxifen treatment. (C-D) frequencies and cell numbers of B220$^+$CD19$^+$ B cells and CD11b$^+$ myeloid cells in the BM of *Ctrl* and CreERT2$^+$*Reg1*$^{fl/fl}$*Reg3*$^{-/-}$ (*DKO*$^{CreERT2}$) mice. n = 6, *Ctrl*; n = 4, *DKO*$^{CreERT2}$. (E) Gating strategy of HSPCs. LT-HSC, Flt3$^-$CD48$^-$CD150$^+$ LSK; ST-HSC, Flt3$^-$CD48$^-$CD150$^-$ LSK; MPP2, Flt3$^-$CD48$^+$CD150$^+$ LSK; MPP3, Flt3$^-$CD48$^+$CD150$^-$ LSK; MPP4, Flt3$^+$CD48$^+$CD150$^-$ LSK; CLP, Lin$^-$Flt3$^+$IL-7Rα$^+$Sca1$^{dull}$Kit$^{dull}$. (F) Cell type distribution of HSPCs in *Ctrl* and *DKO*$^{CreERT2}$ mice. (G) Cell numbers of HSPC subpopulations in *Ctrl* and *DKO*$^{CreERT2}$ mice. Error bars denote the mean ± SD. *p < 0.05; **p < 0.01; ***p < 0.001; ****p < 0.0001. Unpaired two-tailed Student's *t*-test. ns, not significant.

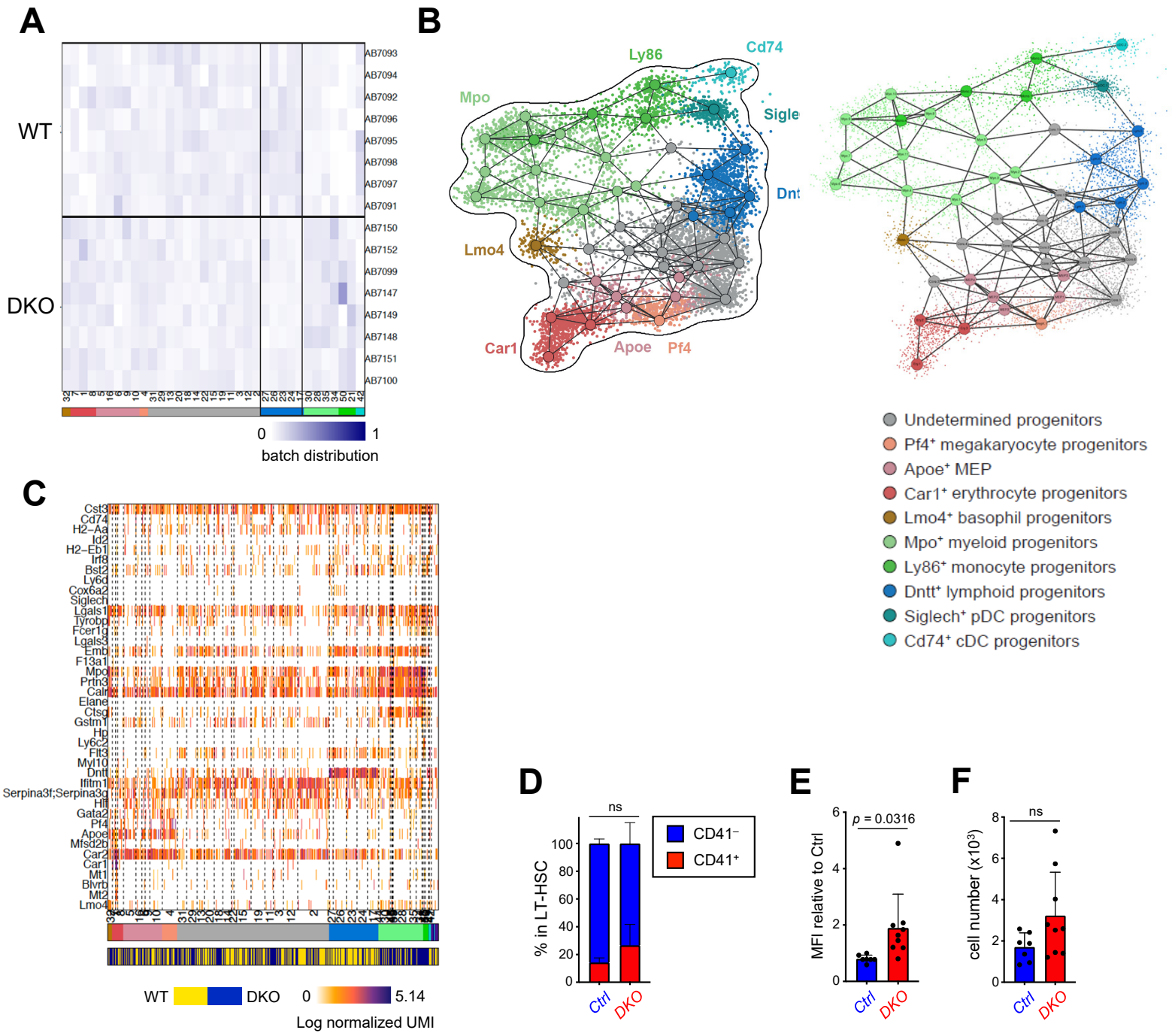


**Supplemental Figure 4. Deletion of *Reg1* and *Reg3* skews gene expression patterns toward myeloid and Meg-E lineage signatures in HSPCs** (A) Enrichment of meta-cell clusters across the 384 plates of WT and DKO cells (eight plates in each genotype). Lower bar indicates meta-cell clusters. (B) A two-dimensional representation of the reference model of the hematopoietic core constructed from 8,395 BM myeloid progenitors grouped into meta-cells (left panel), as reported previously (Giladi et al. 2018). Metacell analysis enables the identification of "meta-cells," which represent smaller subgroups within a cluster sharing similar transcriptional profiles. This methodology helps distinguish between closely related cell types or states that might otherwise be merged into a single cluster when using conventional clustering techniques (Also see supplemental methods). The number of each metacell was depicted in the core map (right panel, also see Supplemental Table S3). Cells are colored by expression of functional markers. (C) Single-cell gene expression profiles. Color bar: upper, annotation of meta-cells (see Methods) and lower, genetic backgrounds (yellow; WT, blue; DKO). (D-F) frequency and MFI of CD41 in LT-HSCs (CD45.2) and cell number of CD41$^+$ LT-HSCs (CD45.2) from competitively transplanted mice. *Ctrl*, n = 7; *DKO*, n = 9. Error bars denote the mean ± SD (D-F). Unpaired two-tailed Student's *t*-test. ns, not significant.

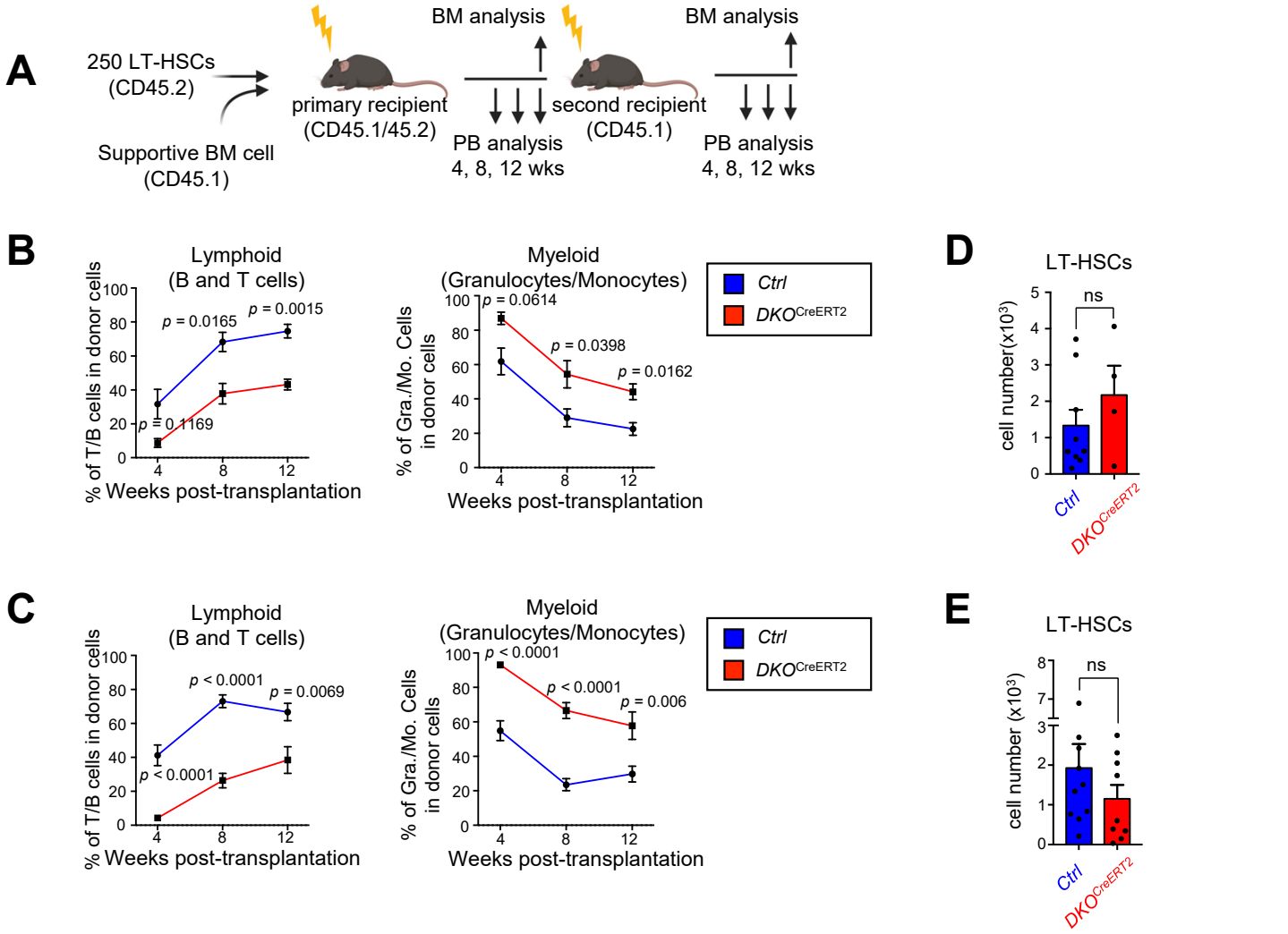


**Supplemental Figure 5. *Reg1/Reg3*-deficient HSCs exhibit myeloid-biased output upon serial transplantation**

(A) Experimental schematic for primary and secondary transplantations. Recipient mice (CD45.1/CD45.2) were lethally irradiated and competitively transplanted with 250 LT-HSCs from *Ctrl* and CreERT2$^{+}$*Reg1*$^{fl/fl}$*Reg3*$^{-/-}$ (*DKO*$^{CreERT2}$) mice (CD45.2) treated with tamoxifen. For secondary transplants, 1 million whole BM cells were transferred from primary recipient mice to secondary recipient mice (CD45.1). (B-C) Reconstitution potential and hematopoietic outputs after primary and second transplantation. Donor-derived lymphoid and myeloid outcomes in the peripheral blood. (D-E) Cell numbers of donor-derived LT-HSCs following primary and secondary transplantation. ((D) *Ctrl*, n = 9; *DKO*$^{CreERT2}$, n = 4) ((E) *Ctrl*, n = 10; *DKO*$^{CreERT2}$, n = 9) Error bars denote the mean ± SD (D, E) or ± SEM (B, C). Unpaired two-tailed Student's *t*-test. ns, not significant.

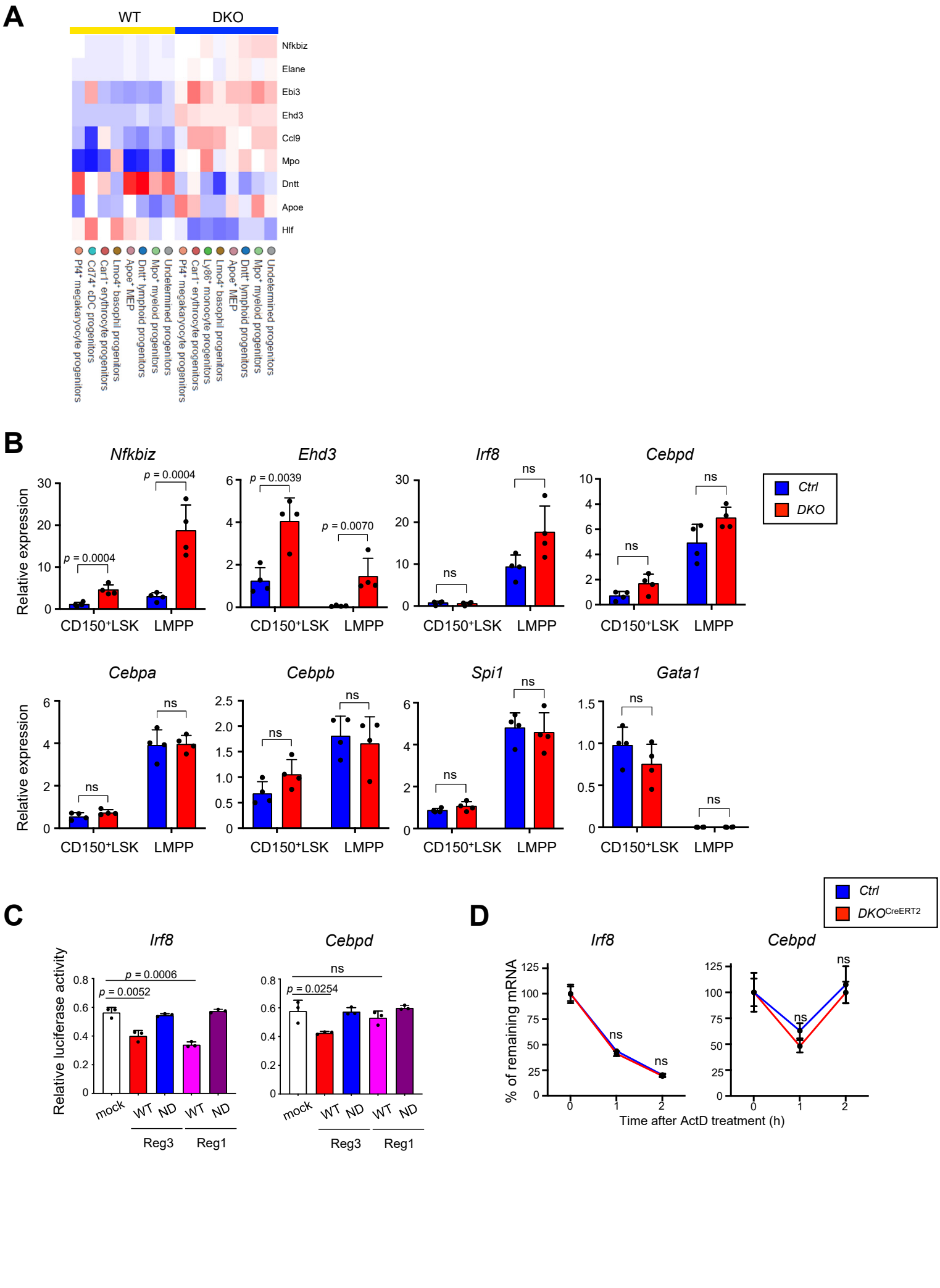
A
WT
DKO
Nfkbiz
Elane
Ebi3
Ehd3
Ccl9
Mpo
Dntt
Apoe
Hlf
Pf4+ megakaryocyte progenitors
Cd74+ cDC progenitors
Car1+ erythrocyte progenitors
Lmo4+ basophil progenitors
Apoe+ MEP
Dntt+ lymphoid progenitors
Mpo+ myeloid progenitors
Undetermined progenitors
Pf4+ megakaryocyte progenitors
Car1+ erythrocyte progenitors
Ly86+ monocyte progenitors
Lmo4+ basophil progenitors
Apoe+ MEP
Dntt+ lymphoid progenitors
Mpo+ myeloid progenitors
Undetermined progenitors
B
Nfkbiz
Ehd3
Irf8
Cebpd
Relative expression
p = 0.0004
p = 0.0004
p = 0.0039
p = 0.0070
ns
CD150+LSK
LMPP
Ctrl
DKO
Cebpa
Cebpb
Spi1
Gata1
C
Irf8
Cebpd
Relative luciferase activity
p = 0.0006
p = 0.0052
p = 0.0254
mock
WT
ND
Reg3
Reg1
D
Ctrl
DKOCreERT2
Irf8
Cebpd
% of remaining mRNA
Time after ActD treatment (h)

**Supplemental Figure 6. Nfkbiz is upregulated in HSPCs lacking *Reg1* and *Reg3*** (A) Heatmap showing the 9 selected genes differentially expressed in DKO cells in the scRNA-seq data (supplemental Figure 4). (B) Expression levels of the indicated genes in $CD150^{+}$ LSK cells and LMPP derived from mice competitively transplanted with wild-type (*Ctrl*, CD45.1) and $Reg1^{-/-}$ $Reg3^{-/-}$ (*DKO*, CD45.2) FL cells. *Ctrl* and *DKO* cells were sorted separately based on congenic markers (n = 4 each). Transcript levels were determined by quantitative RT-PCR. Data are a composite of two independent experiments. (C) Luciferase activity was assessed by using pGL3 plasmids containing 3'UTR of *Irf8* and *Cebpd*, together with mock or plasmids for wild-type or nuclease-dead mutant for Reg1 and Reg3 (n = 3 each). (D) mRNA stability of *Irf8* and *Cebpd* in $Lin^{-}$ cells from control and $DKO^{CreERT2}$ mice. Cells were stimulated with IL-1β for 2 hours, followed by addition of actinomycin D (ActD). The remaining transcripts relative to the 0 h time point were measured by quantitative RT-PCR. Data are representative of two independent experiments (C, D) or a composite of two experiments (A). Data are presented as mean ± SD (A, C) or SEM (D). Statistical significance was calculated by unpaired two-tailed Student's *t*-test. ns, not significant.

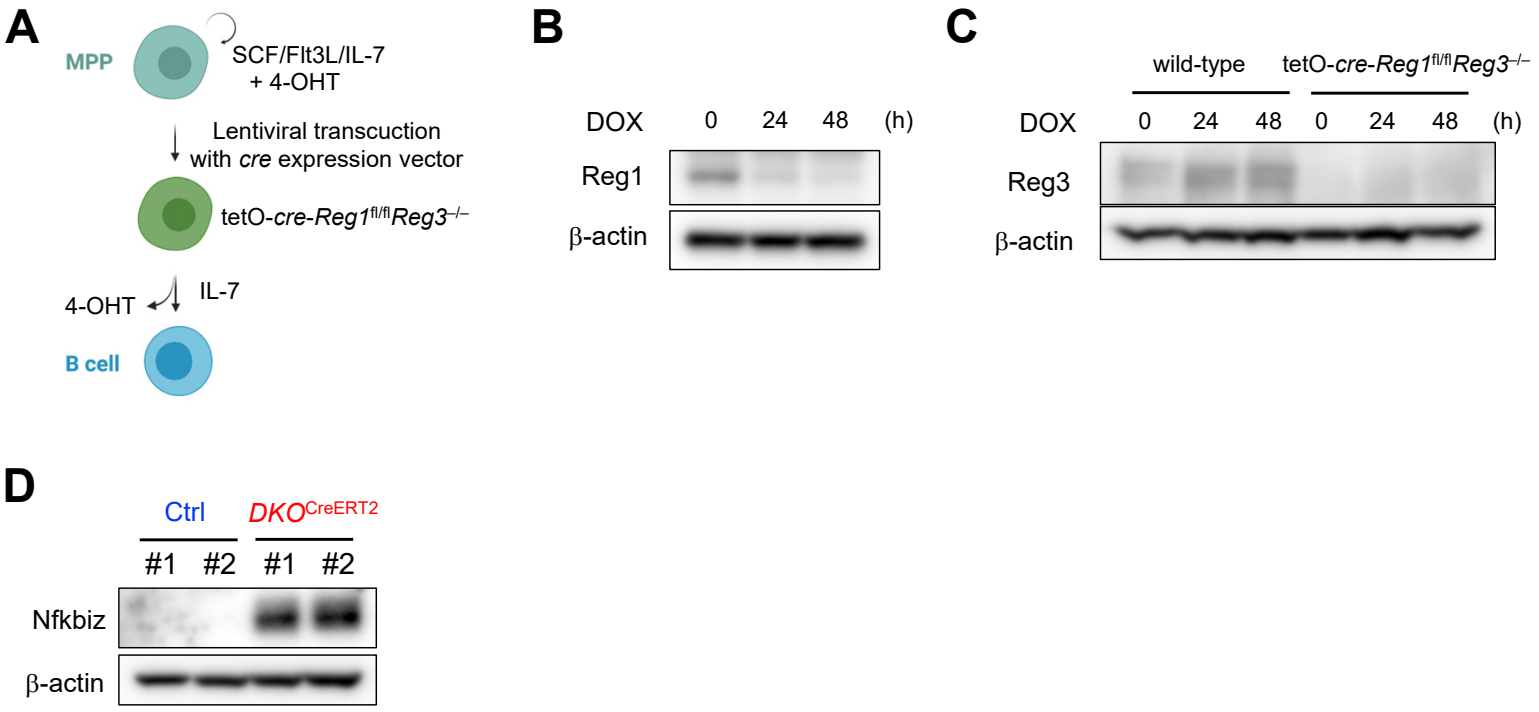


**Supplemental Figure 7. Nfkbiz is upregulated in HSPCs lacking *Reg1* and *Reg3*** (A) (D) Schematic representation for establishment of tetO-*cre-Reg1*$^{fl/fl}$*Reg3*$^{-/-}$ MPP$^{hId3\text{-}ERT2}$ cells. (E-F) Immunoblot analysis of Reg1 and Reg3 in tetO-*cre-Reg1*$^{fl/fl}$*Reg3*$^{-/-}$ MPP$^{hId3\text{-}ERT2}$ cells following addition of DOX. (G) Immunoblot analysis of Nfkbiz in Lin$^{-}$ cells from control and CreERT2$^{+}$*Reg1*$^{fl/fl}$*Reg3*$^{-/-}$ (*DKO*$^{CreERT2}$) mice at day 3 after tamoxifen injection. Data are representative of two independent experiments (B, C, E-G) or a composite of two experiments (A). Data are presented as mean ± SD (A-B) or SEM (C). Statistical significance was calculated by unpaired two-tailed Student's *t*-test. ns, not significant.

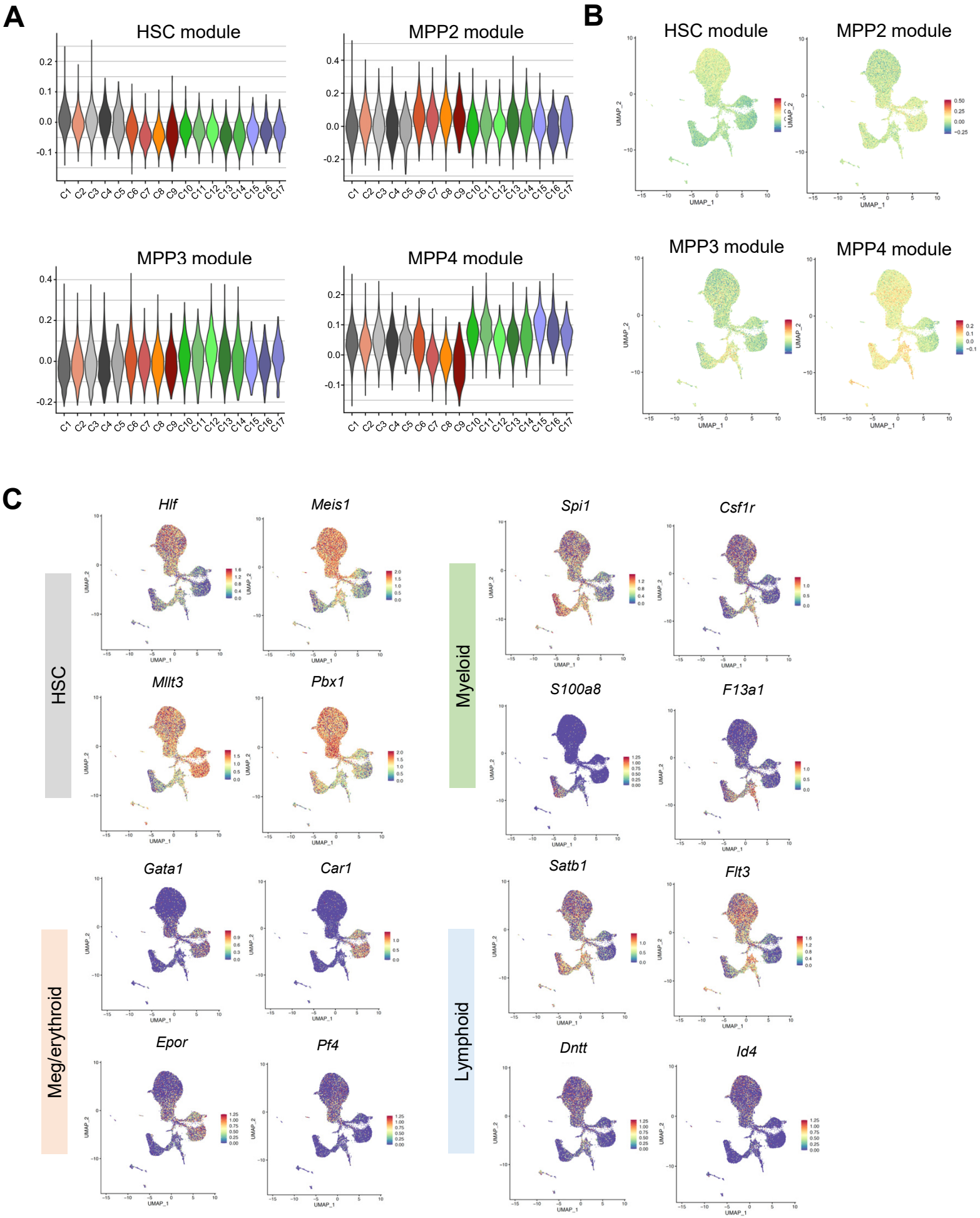
A
HSC module
MPP2 module
MPP3 module
MPP4 module
B
HSC module
MPP2 module
MPP3 module
MPP4 module
C
HSC
Myeloid
Meg/erythroid
Lymphoid
Hlf
Meis1
Spi1
Csf1r
Mllt3
Pbx1
S100a8
F13a1
Gata1
Car1
Satb1
Flt3
Epor
Pf4
Dntt
Id4

**Supplemental Figure 8. Single-cell ATAC-seq generated clusters characterized by distinct patterns of chromatin accessibility in Flt3$^{-}$CD48$^{-}$LSK cells** (A) Violin plots showing the chromatin accessibility of signature gene sets for HSC, MPP2, MPP3, and MPP4 across all scATAC-seq clusters. (B) UMAP plots showing the chromatin accessibility of signature gene sets for HSC, MPP2, MPP3, and MPP4. (C) UMAP plots showing normalized chromatin accessibility of the selected signature genes for stemness and lineage specification.

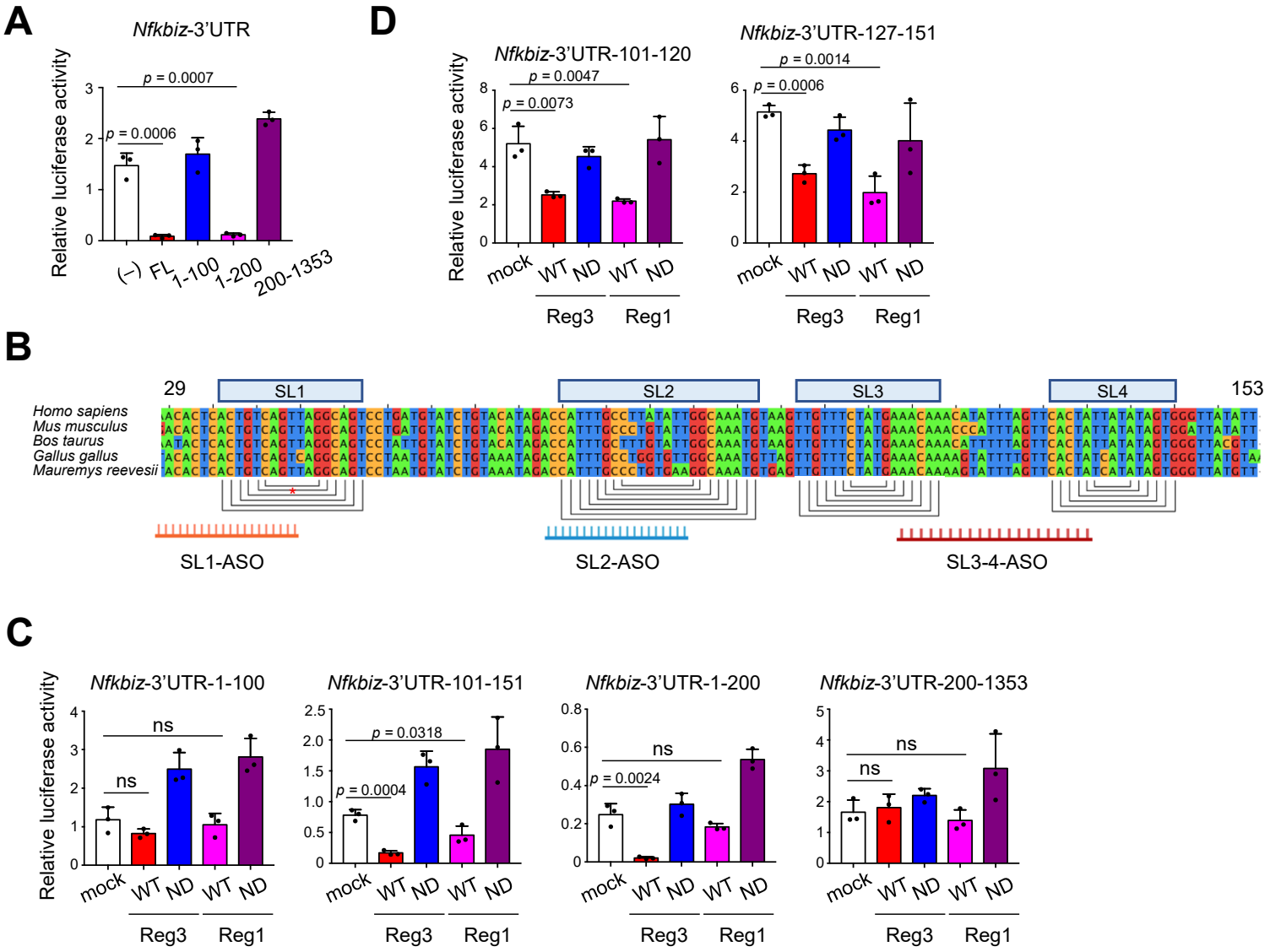


**Supplemental Figure 9. *Nfkbiz*-3'UTR 101-151 region is essential for destabilization by Reg1 and Reg3** (A) Luciferase activity of HeLa cells transfected with pGL3 plasmids containing various lengths of 3'UTR of mouse *Nfkbiz* (n = 3 each). (B) Schematic representation of Reg1/Reg3-recognition sequences and potential SL structures (SL1-4) in mouse *Nfkbiz* together with an alignment of four other species. SL structures were predicted by RNAfold. Single strand oligonucleotides against the indicated SL structures are shown at the bottom. Asterisk indicates a mismatch base pair. (C) Luciferase activity of HeLa cells transfected with pGL3 plasmids containing a set of *Nfkbiz* 3'UTR as in a,, together with expression plasmids for wild-type (WT) or nuclease-dead (ND) mutant of Reg1 and Reg3 (n = 3 each). (D) Luciferase activity of HeLa cells transfected with pGL3-βGlo plasmids containing the 101-120 or 127-151 of *Nfkbiz* 3'UTR together with expression plasmids for WT or ND mutant of Reg1 and Reg3 (n = 3 each). Bar graphs are presented as mean ± SD (A, C, D). Unpaired two-tailed Student's *t*-test. ns, not significant. Data are representative from three independent experiments (A, C, D).

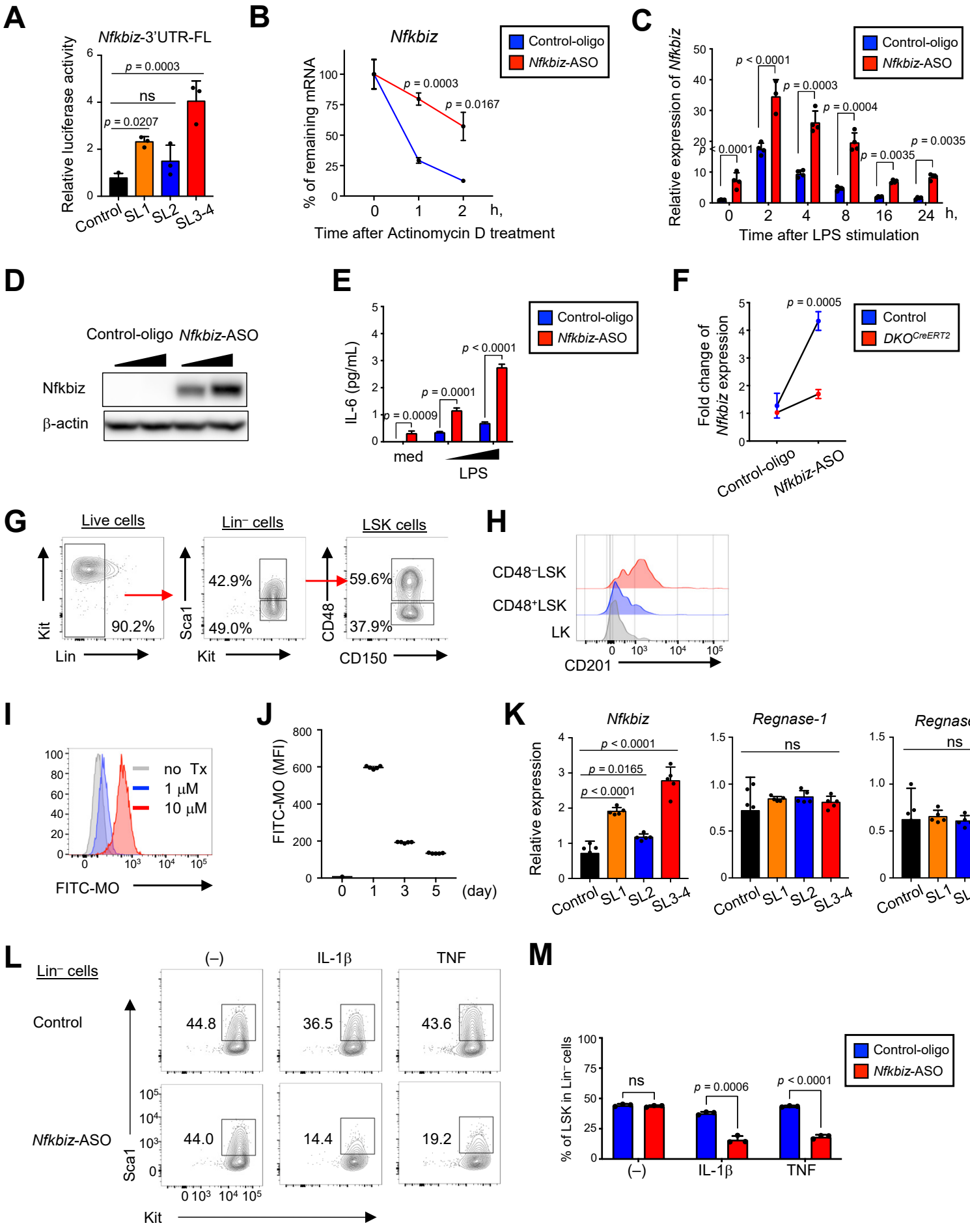
A
Nfkbiz-3'UTR-FL
Relative luciferase activity
p = 0.0003
ns
p = 0.0207
Control
SL1
SL2
SL3-4
B
Nfkbiz
Control-oligo
Nfkbiz-ASO
% of remaining mRNA
p = 0.0003
p = 0.0167
Time after Actinomycin D treatment
C
Relative expression of Nfkbiz
Control-oligo
Nfkbiz-ASO
p < 0.0001
p = 0.0003
p = 0.0004
p = 0.0035
p = 0.0001
p = 0.0035
Time after LPS stimulation
D
Control-oligo
Nfkbiz-ASO
Nfkbiz
β-actin
E
IL-6 (pg/mL)
Control-oligo
Nfkbiz-ASO
p < 0.0001
p = 0.0001
p = 0.0009
med
LPS
F
Fold change of Nfkbiz expression
p = 0.0005
Control
DKOCreERT2
Control-oligo
Nfkbiz-ASO
G
Live cells
Lin⁻ cells
LSK cells
Kit
Lin
90.2%
Sca1
Kit
42.9%
49.0%
CD48
CD150
59.6%
37.9%
H
CD48⁻LSK
CD48⁺LSK
LK
CD201
I
no Tx
1 μM
10 μM
FITC-MO
J
FITC-MO (MFI)
(day)
K
Nfkbiz
Regnase-1
Regnase-3
Relative expression
p < 0.0001
p = 0.0165
p < 0.0001
ns
ns
Control
SL1
SL2
SL3-4
L
Lin⁻ cells
(–)
IL-1β
TNF
Control
Nfkbiz-ASO
44.8
36.5
43.6
44.0
14.4
19.2
Sca1
Kit
M
% of LSK in Lin⁻ cells
Control-oligo
Nfkbiz-ASO
ns
p = 0.0006
p < 0.0001
(–)
IL-1β
TNF

**Supplemental Figure 10. Manipulation of *Nfkbiz* expression modulates lineage bias in HSCs** (A) Luciferase activity of HeLa cells transfected with pGL3 plasmid containing full length of mouse *Nfkbiz* 3'UTR, along with a set of ASOs targeting its stem loop structures (n = 3 in SL1, SL2, and SL3-4). (B) The mRNA stability of *Nfkbiz* transcript was measured by qRT-PCR. 24 hours after transfection with Control oligo or *Nfkbiz*-targeting ASO, bone marrow-derived macrophages (BMDMs) were stimulated with LPS (100 ng/mL) for 2 hours, followed by treatment with actinomycin D (5 μg/mL) for the indicated time points (n = 4 each). (C) qRT-PCR analysis of *Nfkbiz* in BMDMs transfected with Control oligo or *Nfkbiz*-targeting ASO, then stimulated with LPS (100 ng/mL) at the indicated time points (n = 3 each). (D) Immunoblot analysis of Nfkbiz in BMDMs 24 hours after transfection with Control oligo or *Nfkbiz*-targeting ASO. (E) IL-6 production of BMDMs stimulated with LPS (10 or 100 ng/mL). Cells were transfected with ASOs (n = 3 each). (F) Fold change of *Nfkbiz* expression in DKO BMDMs comparing WT cells, transfected with ASOs (n = 3 each). (G) Flow cytometry plots of cultured HSCs. Please refer to Method. (H) Histogram of CD201 expression in $CD48^-$ and $CD48^+$ LSK populations from cultured HSCs. (I, J) Representative histogram of FITC-conjugated morpholino oligonucleotide (MO) in cultured HSCs at 24 hours after electroporation (I). MFI of FITC-MO in cultured HSCs was monitored by flow cytometry at the indicated time points (J) (n = 3 each). (K) quantitative RT-PCR analysis for *Nfkbiz, Reg1,* and Reg3 in cultured HSCs treated with control oligo or SL-targeting ASOs (n = 5 each). (L, M) Representative flow cytometry plots and frequency of LSK population in cultured HSCs 24 hours after electroporation with control oligo or *Nfkbiz*-targeting ASO. Cells were then stimulated with IL-1β (25 ng/mL) or TNF (1 μg/mL) for 24 hours (n = 3 each). Data are presented as mean ± SD (A, C, E, F, K, M) or SEM (B). Statistical significance was calculated by one-way ANOVA with Holm-Sidak multiple comparisons test (A, K) or unpaired two-tailed Student's *t*-test (B, C, E, F, M). ns, not significant. Data are a representative from two independent experiments.

**SUPPLEMENTAL INFORMATION**

**Supplementary Method details**

**Animals**

*Regnase-3*-deficient (*Reg3*$^{-/-}$) mice were generated by CRISPR-Cas9 technology. Guide RNA targeting exon 3 of the *Reg3* locus was injected into zygotes (gRNA sequence: AAAGAAGTATTCTCGTGCCG). *Nfkbiz* flox mice[1] and *Il7rCre R26R-EYFP* mice[2] were kindly provided by T. Maruyama and HR. Rodewald, respectively. *Regnase-1*$^{-/-}$[3] and *Regnase-1* flox [4] mice were bred in our own animal colony. B6.SJL-*Ptprc*$^{a}$ *Pepc*$^{b}$/BoyJ and *R26-CreERT2* mice were originally from the Jackson Laboratory. C57BL/6J mice were purchased from The CLEA Japan. All mice were housed under SPF conditions. All animal experiments were done with the approval of the Animal Research Committee of Graduate School of Medicine, Kyoto University.

**Cell culture and transfection**

HEK293T cells were maintained in DMEM (nacalai tesque) supplemented with 10% fetal bovine serum (FBS) (Clontech). Tet-off HEK293 cells were cultured in α-MEM (nacalai tesque) supplemented with 10% Tet-off system-approved FBS (Takara Bio) and 100 mg/ml G418 (nacalai tesque). Flp-In 293 T-Rex cells (Invitrogen) were grown in DMEM with 10% FBS and 2 mM L-glutamine. TSt-4 stroma cells were cultured in RPMI 1640 (nacalai tesque) supplemented with 10% FBS, 1 mM sodium pyruvate (Gibco), 0.1 mM non-essential amino acids solution (Gibco), 50 mM β-mercaptoethanol (nacalai tesque), 100 U/mL penicillin, and 100 mg/mL streptomycin (nacalai tesque). PEI MAX (Polysciences, Inc) was used for transfection following the manufacturer's protocol. For mRNA decay experiments with Tet-off system, Tet-off 293 cells were transfected with pTRE-tight vectors. Twenty-four hours post-transfection, doxycycline (2 μg/ml) (Sigma) was added to the medium for the indicated time intervals before harvesting cells.

**Flow Cytometry**

Single cell suspensions were prepared from the BM and spleen and resuspended in FACS

buffer (5% BSA, 2mM EDTA in PBS). Single-cell suspensions were prepared and stained with fluorochrome-conjugated antibodies with the following specificities: CD3e (145-2C11), CD4 (GK1.5), CD8a (53-6.7), CD11b (M1/70), CD11c (N418), CD16/CD32 (2.4G2), CD19 (MB19-1), CD25 (PC61), CD34 (HM34), CD41 (MWReg30), CD61 (2C9.G2), CD45.1 (A20), CD45.2 (104), CD45R/B220 (RA3-6B2), CD48 (HM48-1), CD90.1 (HIS51), CD105 (MG7/18), c-Kit (2B8), IL-7Ra (A7R34), CD135 (A2F10), CD150 (TC15-12F12.2), CD201 (RCR-16), Sca-1 (D7), Ly-6D (49-H4), Ly-6G/Ly-6C (RB6-8C5), NK-1.1 (PK136), TCR b chain (H57-597), TER-119 (TER-119). For surface markers, staining was performed for 20 min at four degree. After washed twice, cells were stained with propidium iodide (PI) prior to FACS analysis. Except for staining with CD16/CD32 antibody, rat anti-mouse CD16/CD32 (Mouse BD Fc Block) was used to block FcRs. Stained cells were analyzed on an LSR Fortessa (BD Biosciences) and analyzed using FlowJo software (Tree Star).

For the identification of HSC and MPPs, BM cells were gated on lineage-negative (CD3, CD4, CD8, CD19, B220, CD11b, CD11c, Gr-1, Ter119, NK1.1), $Sca1^{+}$, and $Kit^{+}$ (LSK). In FL transplantation experiments, LSK cells were further separated into $Flt3^{-}CD150^{+}$ LSK and $Flt3^{hi}CD150^{-}$ LMPP. In non-reconstitution mouse models, LSK were further separated into $Flt3^{-}CD150^{+}CD48^{-}$ LT-HSC, $Flt3^{-}CD150^{-}CD48^{-}$ ST-HSC, $Flt3^{-}CD150^{+}CD48^{+}$ MPP2, $Flt3^{-}CD150^{-}CD48^{+}$ MPP3, $Flt3^{+}CD150^{-}CD48^{+}$ MPP4 (Supplemental Figure 3C). CLP was identified as $Flt3^{+}$IL-7R$\alpha^{+}Lin^{-}Sca1^{int\text{-}lo}Kit^{int\text{-}lo}$ population. Pre-GM, GMP, pre-Mk/E, and MkP progenitor populations were identified as $Lin^{-}Sca1^{-}Kit^{+}$ (LK). Pre-GMs were further gated as $CD41^{-}Fc\gamma R^{-}CD105^{-}CD150^{-}$, GMP as $CD41^{-}Fc\gamma R^{+}$CD150–, pre-Mk/E as $CD41^{-}Fc\gamma R^{-}CD105^{-}CD150^{+}$, MkP as $CD41^{+}$. Mature cell populations were defined as following: pro-B cells ($IgM^{-}IgD^{-}CD25^{-}Kit^{+}CD19^{+}B220^{+}$), pre-B cells ($IgM^{-}IgD^{-}CD25^{+}Kit^{-}CD19^{+}B220^{+}$), Immature B cells ($IgM^{+}IgD^{-}CD19^{+}B220^{+}$), mature B cells ($IgM^{+}IgD^{+}CD19^{+}B220^{+}$), granulocytes ($Gr\text{-}1^{hi}CD11b^{+}$), and monocytes ($Gr\text{-}1^{int\text{-}lo}CD11b^{+}$).

**BrdU Incorporation Assay and Annexin V Staining**

For cell proliferation analysis, the BrdU Flow Kit (BD Pharmingen) was used according to the manufacturer's instructions. Mice were intraperitoneally injected with 100 μg of BrdU 1 hour before the analysis. PBS injection was used as a negative control. FACS-sorted populations were stained with anti-BrdU antibodies. For apoptosis analysis, cells were stained with Annexin V (Biolegend) in Annexin buffer (10 mM HEPES (pH7.4), 140 mM NaCl, 2.5 mM $CaCl_2$) along with 7-AAD. Flow cytometric analysis of these cells were performed by using LSR Fortessa (BD Biosciences).

**Reconstitution experiments**

For the generation of full chimeras, FL cells were purified from E15.5 embryos (CD45.2) with the indicated genotypes. Cells were injected intravenously into lethally irradiated (10 Gy) congenic B6.SJL-Ptprc$^{a}$ Pepc$^{b}$/BoyJ (CD45.1) mice. BM cells were analyzed at 4-6 weeks after transplantation. For competitive transplantation, FL cells from CD45.1 WT together with those either from CD45.2 control or *DKO* fetuses were 1:1 mixed and transplanted into lethally irradiated CD45.1/CD45.2 mice. Mice were sacrificed at 4-6 weeks after transplantation. The reconstitution efficiency was more than 95%. Cells were prepared from BM, thymus, and peripheral blood, and used for further experiments. For HSC reconstitution assays, CD45.1/CD45.2 recipient mice were lethally irradiated prior to transplantation (4.5 Gy × 2). 250 Flt3$^{-}$CD48$^{-}$CD150$^{+}$ LSK (LSK-SLAM) cells were sorted from CD45.2 CreERT2$^{+}$*Reg1*$^{fl/+}$*Reg3*$^{+/-}$ or CreERT2$^{+}$*Reg1*$^{fl/fl}$*Reg3*$^{-/-}$ mice 14 days after tamoxifen treatment and then transplanted into the recipient mice together with 5 × $10^5$ supportive total BM cells. For secondary transplantations, 1 × $10^6$ total BM cells were isolated and transplanted into lethally irradiated secondary recipients (CD45.1) (4.5 Gy × 2). Contribution of CD45.2 donor cells was monitored in peripheral blood every 4 weeks post transplantation using LSR Fortessa (BD Biosciences). Peripheral blood collections for assessment of donor chimerism were performed at 4, 8, and 12 weeks after primary and secondary transplantations. Cells were stained with antibodies to CD45.1, CD45.2,

CD11b, Gr-1, B220, CD19, CD4, CD8, and TCR-b. Recipients with lower than 1% total chimerism were considered failed transplantations and excluded from analysis.

**BM Preparation and Lineage Depletion**

BM cells were purified from femurs, tibias, humeruses and ilia by crushing bones with mortar and pestle in sterile PBS (nacalai tesque) supplemented with 2% BSA and 1mM EDTA. Red blood cells were lysed in BM cells with ACK lysing buffer (Thermo Fisher Scientific). $Lin^-$ cells or $Kit^+$ cells were purified using Lineage Cell Depletion Kit or anti-PE MicroBeads (Miltenyi Biotec) on LS MACS columns (Miltenyi Biotec). Cells were then used for subsequent experiments or sorted on FACSAria III cell sorter (BD Biosciences).

**Establishment of $MPP^{hId3\text{-}ERT2}$ Cells**

Id3-ERT2-expressing multipotent progenitor ($MPP^{hId3\text{-}ERT2}$) cells were established as described previously.[5] Briefly, LSK cells were purified from BM of WT or *Reg1*$^{fl/fl}$*Reg3*$^{-/-}$*ROSA*$^{yfp/+}$ mice, then retrovirally transduced with the plasmid expressing hId3-ERT2-IRES-GFP by spin-infection. Cells were cultured on TSt-4 stromal cells in IMDM (Gibco) supplemented with 10 ng/mL mSCF, 10 ng/mL mFlt3L, and 20 ng/mL mIL-7 (R&D) and 40 nM 4-OHT (Sigma). For B cell differentiation, cells were cultured on TSt-4 cells in IMDM supplemented with 5 ng/mL mIL-7 in the absence of 4-OHT. For in-vitro doxycycline-inducible cre expression, $MPP^{hId3\text{-}ERT2}$ cells were lentivirally transduced with pInducer20-tagBFP containing cre sequence, and treated with 2 μg/mL doxycycline. For RNA-immunoprecipitation (RIP)-RT-qPCR assay, these cells were transduced with pInducer20-mCherry containing either FLAG-tagged Reg1 or Reg3. For retroviral overexpression, $MPP^{hId3\text{-}ERT2}$ cells were transduced with MSCV-Thy1.1 by spin infection. The infected cells were washed twice and cultured on TSt-4 cells for 6 days under B cell-differentiating condition.

***Ex vivo* HSC culture**

*Ex-vivo* HSC serum-free culture was performed as described previously.[6] Soluplus®

(polyvinyl caprolactam-polyvinyl acetate-polyethylene glycol graft copolymer) was kindly provided by S. Yamazaki.[7] Briefly, $Kit^+$ cells were isolated from the bone marrow of C57BL/6 mice by using anti-PE MicroBeads (Miltenyi Biotec). Cells were cultured in serum-free F12 medium (Life Technologies), supplemented with SCF (10 ng/mL; PeproTech), TPO (100 ng/mL; PeproTech), Insulin-Transferrin-Selenium-Ethanolamine (ITSX; 1%; Life Technologies), HEPES (10 mM; Gibco), and with Soluplus (0.1%). Media changes were performed three times a week. HSC quality was monitored by flow cytometry based on the expression of CD150, CD48, and CD201 in LSK population. For HSC stimulation, IL-1β or TNF were added at 25 ng/mL or 1 mg/mL, respectively.

**Measurement of Lymphoid Lineage Potential**

B lymphocyte potential of purified progenitors was evaluated following co-culture on TSt-4 stromal cells. $Lin^-Kit^+IL\text{-}7R\alpha^+$ cells were purified from FL cells at E16.5. Cells were then seeded onto stroma monolayers in 24-well plates and cultured in RPMI supplemented with 10 ng/mL mSCF, 10 ng/ml mFlt3L, and 10 ng/ml mIL-7 (Peprotech). For induction of cre recombinase, 4-OHT was added at 40 nM. On day 6 or day 7, cells were subjected to flow cytometry to assess generation of $CD19^+$ B cells and $CD11b^+$ myeloid cells.

**Luciferase assay**

HEK293 or HeLa cells were transfected with mock or pGL3 plasmids containing various 3'UTR (listed in Supplementary Table S6), together with mock or expression plasmids for Reg1 and Reg3. After 24 h of cultivation, luciferase activities in the lysates were determined using the Dual-luciferase reporter assay system (Promega), according to the manufacturer's protocol. The Renilla luciferase gene was simultaneously transfected as an internal control.

**Immunoblot analysis**

Whole-cell lysates were prepared in lysis buffer (1% (vol/vol) Nonidet P-40, 0.1% (wt/vol) SDS, 1% (wt/vol) sodium deoxycholate, 150mM NaCl, 20mM Tris-HCl, pH7.5,

and 1mM EDTA), supplemented with Complete Mini Protease Inhibitor Cocktail without EDTA (Roche)). Lysates were separated by SDS-PAGE and transferred to nitrocellulose membranes (BIO RAD). The following antibodies were used for immunoblot analysis: antibody against IκB-ζ (14-6801-80; Thermo), FLAG-tag (F3165; Sigma) or antibody against β-actin (sc-1615; Santa Cruz) serving as a loading control. Polyclonal rabbit Regnase-1 and monoclonal rat anti-Regnase-3 (4D3) antibodies were previously described.[8,9] Luminescence was detected with a luminescent image analyzer (ImageQuant LAS 4000; GE Healthcare).

**Quantitative RT-PCR Analysis**

Total RNA was isolated using TRIzol (Thermo Fisher Scientific) or Dynabeads MyOne Silane (Thermo Fisher Scientific). Reverse-transcription (RT) was carried out using ReverTra Ace® qPCR RT Master Mix with gDNA Remover (TOYOBO) or SuperScript IV VILO Master Mix (Thermo Fisher Scientific). Quantitative PCR (qPCR) was performed with SYBR® Select Master Mix (Applied Biosystems). Fluorescence was detected with a StepOne Real-Time PCR System (Applied Biosystems). qPCR primers used are listed in supplemental Table 5.

**mRNA stability**

Actinomycin D (5 μg/ml) was added directly to cell cultures following treatment with IL-1β or LPS for 2 hours. Cells were harvested at the indicated time after the addition of actinomycin D, followed by RT-qPCR analysis of mRNA as described above.

**RNA-immunoprecipitation (RIP)-RT-PCR**

Cells were washed in PBS and lysed in 1mL RNA IP lysis buffer (50 mM Tris-HCl, [pH 7.5], 150 mM KCl, 2 mM EDTA [pH 8.0], 0.5% NP-40, 0.5 mM DTT, complete EDTA-free protease inhibitor cocktail (Roche) and 0.2 U/ml RNasin (Promega)). After incubation on ice for 10 min, followed by centrifugation, 5% of the total lysates were stored for input RNA and immunoblot analysis. FLAG-conjugated Protein G magnetic beads (Thermo Fisher Scientific) were incubated with the lysates for 3 hours at 4 ºC.

Beads were washed three times in RNA IP lysis buffer (50 mM Tris-HCl, [pH 7.5], 150 mM KCl, 0.5%, NP-40, 0.5 mM DTT and complete EDTA-free protease inhibitor cocktail (Roche)). RNA was eluted by adding RLT buffer (QIAGEN) directly to the beads, then extracted following the instructions of the manufacturer. RIP transcript levels were normalized to input transcript levels and enrichments calculated relative to 18S or RPL18A.

**ASO Delivery**

For delivery of antisense morpholino oligonucleotides, HeLa cells or BM-derived macrophages were seeded in 24 well plate prior to transfection. Morpholinos were added to the medium at a final concentration of 2 μM, followed by addition of 6 μM Endo-Porter (Gene Tools, LLC). For luciferase assay, HeLa cells were transfected with pGL3 plasmid simultaneously using Lipofectamine LTX (Thermo Fisher Scientific). For the delivery of morpholinos into cultured HSCs, electroporation was performed using P3 Primary Cell 4D-Nucleofector™ X Kit (protocol # EO-100, Lonza Bioscience).

**HITS-CLIP**

Flp-In 293 T-REx cell lines stably expressing FLAG/HA-tagged Reg3 were generated as previously described.[10] Expression of epitope-tagged proteins was induced by addition of 1 μg/mL doxycycline. The expression of FLAG/HA-tagged Reg3 protein was assessed by immunoblot analysis using mouse anti-HA antibody (Covance). HITS-CLIP was performed essentially as described.[11] Briefly, UV-irradiated cells were lysed in NP-40 lysis buffer (50 mM HEPES-KOH at pH 7.4, 150 mM KCl, 2 mM EDTA, 0.5% (v/v) NP-40, 0.5 mM DTT, complete EDTA-free protease inhibitor cocktail). After treatment with RNaseT1 (Thermo Fisher Scientific) at final concentration of 0.5 unit/μL, immunoprecipitation was carried out with FLAG magnetic beads (SIGMA) from HEK293 cell extracts for 1 h at 4ºC. Following additional digestion by RNase T1 at final concentration of 0.5 unit/μL, beads were incubated with calf intestinal phosphatase (NEB) and RNA fragments were radioactively end-labeled using T4 polynucleotide

kinase (Thermo Fisher Scientific). The crosslinked protein-RNA complexes were resolved on a 4-12% NuPAGE gel (Invitrogen). The SDS-PAGE gel was transferred to a nitrocellulose membrane (Whatman) and the protein-RNA complex migrating at an expected molecular weight was excised. RNA was isolated by Proteinase K (Roche) treatment and phenol-chloroform extraction, ligated to 3′ adapter and 5′ adapter, reverse transcribed and PCR-amplified. The amplified cDNA was sequenced on a HighSeq2000 (Illumina) with a 1 × 51 nt cycle.

**Massively parallel single-cell RNA sequencing library preparation**

Single-cell libraries were prepared as previously described.[12,13] Briefly, mRNA from cells sorted into cell capture plates was barcoded, converted to cDNA and pooled with an automated pipeline. The pooled sample was then linearly amplified by T7 in vitro transcription, and the resulting RNA was fragmented and converted to a sequencing-ready library by tagging the samples with pool barcodes and Illumina sequences during ligation, reverse transcription and PCR. Each pool of cells was tested for library quality, and the concentration was assessed as described. All RNA-seq libraries (pooled at equimolar concentrations) were sequenced on the Illumina NextSeq 500 platform at a median sequencing depth of 27,994 reads per cell. Sequences were mapped to the mouse genome (mm10), demultiplexed and filtered as described,[12] extracting a set of unique molecular identifiers that defined distinct transcripts in single cells for further processing. We estimated the level of spurious UMIs in the data with statistics on empty MARS-seq wells and excluded all plates with estimated noise of >5%. Mapping of reads was done with HISAT (v0.1.6); reads with multiple mapping positions were excluded. Reads were associated with genes if they were mapped to an exon, using the UCSC Genome Browser for reference. Exons of different genes that shared a genomic position on the same strand were considered to represent a single gene with a concatenated gene symbol. Cells with fewer than 500 UMIs were discarded from the analysis.

**Construction of reference model**

Construction of the hematopoietic core reference models was done by the MetaCell package as previously described and deposited in the GitHub (https://github.com/MetaCell).[14,15] The MetaCell pipeline was used to derive informative genes and compute cell-to-cell similarity, to compute k-nearest neighbor (k-nn) graph covers and derive distribution of RNA in cohesive groups of cells (or meta-cells), and to derive strongly separated clusters using bootstrap analysis and computation of graph covers on resampled data. The hematopoietic core dataset was extracted from cells sorted from four sorting strategies enriching for Kit, Sca-1 and CD150, and depleting different groups of lineage markers. Cells were filtered for high expression of gene sets of the following excluded lineages: ILC (*Ccl5*), megakaryocytes (*Pf4*), erythrocytes (*Car1* and *Hba-a2*), basophils (*Prss34*) and eosinophils (*Prg2*), B cells (*Vpreb1* and *Fcrla*), neutrophils (*Ltf* and *Fcnb*), macrophages (*C1qb*), and DC (*Cd74* and *Siglech*). This resulted in filtering 7,075 cells and retaining 9,348 cells for further analysis. Clustering was performed using MetaCell analysis (but excluding specifically the strong neutrophil differentiation module, including *Camp*, *Ltf*, *S100a8*, *S100a9*, and the hemoglobin genes *Hba-a2*, *Hbb-b1* and *Beta-s*), using bootstrap to derive robust clustering (resampling 70% of the cells in each iteration, and clustering the co-cluster matrix with minimal cluster size set to 20, and number of bootstrap clusters set to 50).

**Projection of sorted cells**

LSK cells from WT and *DKO* mice were projected onto the hematopoietic core reference model as described below. Projected cells were filtered for high expression of gene sets of the following excluded lineages: ILC (*Ccl5*), megakaryocytes (*Pf4*), erythrocytes (*Car1* and *Hba-a2*), basophils (*Prss34*) and eosinophils (*Prg2*), B cells (*Vpreb1* and *Fcrla*), neutrophils (*Ltf* and *Fcnb*), macrophages (*C1qb*), and DC (*Cd74* and *Siglech*), retaining 2241 WT and 2242 *DKO* cells. We extracted for each projected cell the 10 reference cells with top Pearson's correlation over the normalized gene features defined for the reference model. The distribution of cluster memberships over these k-neighbors

was used to associate the new cell with a reference meta-cell (by majority voting) and to project the cell in two dimensions by weighted average of the linked reference clusters' mapped x and y coordinates. To exclude the possibility of variations that might have occurred between the sorting plates of WT and *DKO*, no significant difference in the distribution of meta-cells between the sorting plates was confirmed (supplemental Figure 5A).

**scATAC-seq**

Flt3$^{-}$CD48$^{-}$ LSK cells were sorted as described above. Nuclei isolation for scATAC-seq was performed according to the "Nuclei Isolation for Single Cell ATAC Sequencing Demonstrated Protocol" (10x Genomics). After nuclei isolation, nuclei pellet was suspended in 1× Nuclei Buffer (10x Genomics) and used according to the Chromium Single Cell ATAC Reagent Kits User Guide (10x Genomics). Briefly, nuclei suspensions were incubated in the tagmentation mix for 1 hour at 37 °C. After mixing with a barcoding mix, the nuclei were loaded into a 10x chip H together with barcoded beads and partitioning oil (Chromium Next GEM Chip H Single Cell Kit v1.1, Chromium Next GEM Single Cell ATAC Library & Gel Bead Kit v1.1, 10x Genomics) and encapsulated using the Chromium controller (10x Genomics). The Gel Bead-In Emulsions (GEMs) was transferred into a PCR tube and amplified for 12 cycles in a thermocycler. The barcoded DNA was purified and subjected to an index PCR for 9 cycles. The library amplification was assessed using High Sensitivity DNA chip (Agilent) and sequenced on an Illumina NovaSeq 6000 system using S1 Reagent Kit v1.5 (100cycles) in PE mode (50 × 8 × 16 × 50 read lengths).

**Analysis of scATAC-seq data**

scATAC-seq base call files (BCLs) for each sample were processed into FASTQ files and count data using cellranger-atac mkfastq and cellranger-atac count, as provided by 10x Genomics (version 2.0.0). Data for the four samples were merged using cellranger-atac aggr. Mouse reference data was obtained from the 10x Genomics website (version mm10-

2020-A-2.0.0). The thus obtained feature-to-barcode count matrix and fragment data was further analyzed using the R packages, Seurat (version 4.1.0),[16] Signac (version 1.5.0),[17] EnsDb.Mmusculus.v75 (version 2.99.0)[18]. Peaks present in fewer than ten cells, and cells with fewer than 200 peaks were removed, resulting in a dataset of 195,171 peak loci and 41,606 cells. Additional filtering was performed as follows: we filtered out cells with < 3,000 or > 20,000 fragments inside peak regions, cells with < 30% of fragments inside peak regions, cells with a nucleosome signal > 4 (function NucleosomeSignal), and cells with a TSS enrichment score < 2 (function TSSEnrichment). This resulted in a dataset of 35,160 remaining cells. Normalization was performed using term frequency-inverse document frequency normalization (function RunTFIDF). Linear dimensionality reduction was performed by using singular value decomposition (function RunSVD) on all peak regions, followed by non-linear dimensionality reduction using uniform manifold approximation and projection (UMAP, function RunUMAP) based on the 2$^{nd}$ to 30$^{th}$ latent semantic indexing (LSI) components. The first LSI component was omitted because it was strongly anticorrelated with sequencing depth (function DepthCor). Clustering of cells was performed using the functions FindNeighbors (using the 2$^{nd}$ to 30$^{th}$ LSI) and FindClusters using the smart local moving (SLM) algorithm.

The chromatin accessibility of genes was estimated using the GeneActivity function, which sums the fragments inside the gene body and promoter region (upstream 2kb) of every gene, followed by normalization of this data (function NormalizeData using the total fragment count in each cell as a scale factor, and otherwise default parameters). Accessibility in genomic regions were visualized using function CoveragePlot. Differentially accessible regions (DARs) between clusters were predicted using the FindMarkers function (parameter test.use set to 'LR' and otherwise default parameters). For the prediction between C7 and C8 additional parameters min.pct and logfc.threshold were set to 0.05 and 0.1 respectively.

Enrichment of transcription factor binding site (TFBS) motifs in sets of DARs

was analyzed using R packages JASPAR2020 (version 0.99.10)[19], TFBSTools (version 1.32.0)[20], and BSgenome.Mmusculus.UCSC.mm10 (version 1.4.3)[21]. TFBS motif data was added to the Seurat object using the functions getMatrixSet and Addmotifs, and enriched motifs were predicted using the FindMotifs function. To avoid biases caused by differences in GC content, we used function AccessiblePeaks and MatchRegionStats to define a set of peak regions for generating reference sets with matched GC content, which was given as input to the FindMotifs function.

Gene Ontology (GO) term enrichment analysis was performed as follows. Genes located closest to DARs (with avg_log2FC > 0.2) were picked up using function ClosestFeature, and given as input to the R package GOstats (version 2.60.0)[22]. As gene universe we used all genes in the Seurat object. Genes were converted to Entrez ids using annotation data in R package org.Mm.eg.db (version 3.14.0)[23], and enriched GO terms were predicted using the function hyperGTest. The codes used for the analysis of scATAC-seq data were deposited in the GitHub (https://github.com/alexisvdb/Uehata_scATAC).

**Statistical Analysis**

The variations of data were presented as the means with standard deviations (SDs) or standard errors of the mean (SEMs). A $p$ value of $< 0.05$ was considered significant. For comparison of two groups, a two-tailed unpaired Student's *t*-test for parametric variables was used. For comparisons of multiple groups, one-way ANOVA followed by the Holm-Sidak-corrected two-tailed *t*-tests was used. The statistical analysis indicated in the figure legends were performed with GraphPad Prism Software (GraphPad Inc., La Jolla, CA).

Additional information about experimental procedures is presented in the Supplemental information.

**References**

1. Okuma A, Hoshino K, Ohba T, et al. Enhanced apoptosis by disruption of the STAT3-IkappaB-zeta signaling pathway in epithelial cells induces Sjogren's syndrome-like autoimmune disease. *Immunity*. 2013;38(3):450-460.

2. Schlenner SM, Madan V, Busch K, et al. Fate mapping reveals separate origins of T cells and myeloid lineages in the thymus. *Immunity*. 2010;32(3):426-436.

3. Matsushita K, Takeuchi O, Standley DM, et al. Zc3h12a is an RNase essential for controlling immune responses by regulating mRNA decay. *Nature*. 2009;458(7242):1185-1190.

4. Uehata T, Iwasaki H, Vandenbon A, et al. Malt1-induced cleavage of regnase-1 in CD4(+) helper T cells regulates immune activation. *Cell*. 2013;153(5):1036-1049.

5. Ikawa T, Masuda K, Huijskens M, et al. Induced Developmental Arrest of Early Hematopoietic Progenitors Leads to the Generation of Leukocyte Stem Cells. *Stem Cell Reports*. 2015;5(5):716-727.

6. Wilkinson AC, Ishida R, Kikuchi M, et al. Long-term ex vivo haematopoietic-stem-cell expansion allows nonconditioned transplantation. *Nature*. 2019;571(7763):117-121.

7. Becker HJ, Ishida R, Wilkinson AC, et al. A Single Cell Cloning Platform for Gene Edited Functional Murine Hematopoietic Stem Cells. *bioRxiv*. 2022:2022.2003.2023.485423.

8. Iwasaki H, Takeuchi O, Teraguchi S, et al. The IkappaB kinase complex regulates the stability of cytokine-encoding mRNA induced by TLR-IL-1R by controlling degradation of regnase-1. *Nat Immunol*. 2011;12(12):1167-1175.

9. von Gamm M, Schaub A, Jones AN, et al. Immune homeostasis and regulation of the interferon pathway require myeloid-derived Regnase-3. *J Exp Med*. 2019;216(7):1700-1723.

10. Mino T, Murakawa Y, Fukao A, et al. Regnase-1 and Roquin Regulate a Common Element in Inflammatory mRNAs by Spatiotemporally Distinct Mechanisms. *Cell*. 2015;161(5):1058-1073.

11. Hafner M, Landthaler M, Burger L, et al. Transcriptome-wide identification of RNA-binding protein and microRNA target sites by PAR-CLIP. *Cell*. 2010;141(1):129-141.

12. Jaitin DA, Kenigsberg E, Keren-Shaul H, et al. Massively parallel single-cell RNA-seq for marker-free decomposition of tissues into cell types. *Science*. 2014;343(6172):776-779.

13. Keren-Shaul H, Kenigsberg E, Jaitin DA, et al. MARS-seq2.0: an experimental and analytical pipeline for indexed sorting combined with single-cell RNA sequencing. *Nat Protoc*. 2019;14(6):1841-1862.

14. Giladi A, Paul F, Herzog Y, et al. Single-cell characterization of haematopoietic progenitors and their trajectories in homeostasis and perturbed haematopoiesis. *Nat Cell Biol*. 2018;20(7):836-846.

15. Baran Y, Bercovich A, Sebe-Pedros A, et al. MetaCell: analysis of single-cell RNA-seq data using K-nn graph partitions. *Genome Biol*. 2019;20(1):206.

16. Hao Y, Hao S, Andersen-Nissen E, et al. Integrated analysis of multimodal single-cell data. *Cell*. 2021;184(13):3573-3587 e3529.

17. Stuart T, Srivastava A, Madad S, Lareau CA, Satija R. Single-cell chromatin state analysis

with Signac. *Nat Methods*. 2021;18(11):1333-1341.

18. Rainer J (2017). *EnsDb.Mmusculus.v75: Ensembl based annotation package*. R package version 2.99.0.

19. Fornes O, Castro-Mondragon JA, Khan A, et al. (2019). JASPAR 2020: update of the open-access database of transcription factor binding profiles. Nucleic Acids Res. *48*, D87-D92.

20. Tan G, Lenhard B (2016). "TFBSTools: an R/Bioconductor package for transcription factor binding site analysis." *Bioinformatics*, **32**, 1555-1556.

21. Team TBD (2021). *BSgenome.Mmusculus.UCSC.mm10: Full genome sequences for Mus musculus (UCSC version mm10, based on GRCm38.p6)*. R package version 1.4.3.

22. Falcon S, Gentleman R (2007). "Using GOstats to test gene lists for GO term association." *Bioinformatics*, **23**(2), 257-8.

23. Carlson M (2019). *org.Mm.eg.db: Genome wide annotation for Mouse*. R package version 3.8.2.

Supplemental Table 4. Significant overlap between Reg1 and Reg3 HITS-CLIP peaks

| RBP1 | | RBP2 | | Number 3'UTR | Number of peaks RBP1 | Number of peaks RBP2 | Observed Overlap | Expected Overlap | P-value | Z-score | Fold Enrichment |
|---|---|---|---|---|---|---|---|---|---|---|---|
| Reg1 | replicate1 | Reg3 | replicate1 | 5894 | 683 | 8605 | 106 | 9.94 | 1E-212 | 31.1 | 10.7 |
| Reg1 | replicate1 | Reg3 | replicate2 | 3680 | 683 | 4750 | 47 | 7.71 | 1E-45 | 14.2 | 6.10 |
| Reg1 | replicate2 | Reg3 | replicate1 | 6670 | 3157 | 8605 | 435 | 44.243 | 1E-767 | 59.4 | 9.83 |
| Reg1 | replicate2 | Reg3 | replicate2 | 4901 | 3157 | 4750 | 193 | 29.744 | 1E-210 | 31.0 | 6.49 |